



CHORUS

This is the accepted manuscript made available via CHORUS. The article has been published as:

Thermodynamically consistent incorporation of entanglement spatial fluctuations in the slip-link model

Rudi J. A. Steenbakkers, Marat Andreev, and Jay D. Schieber

Phys. Rev. E **103**, 022501 — Published 3 February 2021

DOI: [10.1103/PhysRevE.103.022501](https://doi.org/10.1103/PhysRevE.103.022501)

Thermodynamically consistent incorporation of entanglement spatial fluctuations in the slip-link model

Rudi J.A. Steenbakkers,^{1,2,*} Marat Andreev,^{1,3,†} and Jay D. Schieber^{1,2,3,4,‡}

¹*Center for Molecular Study of Condensed Soft Matter, Illinois Institute of Technology,
3440 South Dearborn Street, Chicago, Illinois 60616, USA*

²*Department of Chemical and Biological Engineering,
Illinois Institute of Technology, 10 West 35th Street, Chicago, Illinois 60616, USA*

³*Department of Physics, Illinois Institute of Technology,
3101 South Dearborn Street, Chicago, Illinois 60616, USA*

⁴*Department of Applied Mathematics, Illinois Institute of Technology,
10 West 32nd Street, Chicago, Illinois 60616, USA*

(Dated: October 12, 2020)

We evaluate the thermodynamic consistency of the anisotropic mobile slip-link model for entangled flexible polymers. The level of description is that of a single chain, whose interactions with other chains are coarse-grained to discrete entanglements. The dynamics of the model consist of the motion of entanglements through space and of the chain through the entanglements, as well as the creation and destruction of entanglements, which are implemented in a mean-field way. Entanglements are modeled as discrete slip-links, whose spatial positions are confined by quadratic potentials. The confinement potentials move with the macroscopic velocity field, hence the entanglements fluctuate around purely affine motion. We allow for anisotropy of these fluctuations, described by a set of shape tensors. By casting the model in the GENERIC (general equation for the nonequilibrium reversible-irreversible coupling) form of nonequilibrium thermodynamics, we show that (i) since the confinement potentials contribute to the chain free energy, they must also contribute to the stress tensor, (ii) these stress contributions are of two kinds: one related to the “virtual springs” connecting the slip-links to the centers of the confinement potentials and the other related to the shape tensors, and (iii) these two kinds of stress contributions cancel each other if the confinement potentials become anisotropic in flow according to a lower-convected evolution of the confinement strength, or equivalently an upper-convected evolution of the shape tensors of the entanglement spatial fluctuations. In previous publications, we have shown that this cancellation is necessary for the model to obey the stress-optical rule and the Green-Kubo relation, and simultaneously to agree with plateau modulus predictions of multi-chain models and simulations.

I. INTRODUCTION

According to current understanding of polymer liquids, above a certain molecular weight, their response to externally applied stress or strain is dominated by persistent topological constraints, known as entanglements, which result from the fact that polymer chains cannot pass through each other [1–4]. This concept has been the starting point of many attempts to develop predictive, yet tractable rheological models for polymer liquids. There are several molecular models that take a single-chain mean-field level of description [5]. Most of them can be classified either as tube models, in which the collective effect of entanglements is mimicked by a tube that restricts lateral motion of the chain, or as slip-link models, in which each entanglement is described as a discrete object, a slip-link, through which the chain must pass. These models are typically coarse-grained to the level of

the primitive path (PP), i.e., the tube axis in tube models or the shortest path connecting the chain ends through successive entanglements in slip-link models. This means that dynamic processes on length scales smaller than the entanglement spacing are not resolved, and are assumed to be equilibrated.

In a melt or concentrated solution, each monomer has interactions with monomers of other chains. However, according to entanglement theories, only a small subset of all interchain interactions are sufficiently long-lived to affect the stress on a relevant time scale: they make up the persistent topological constraints called entanglements. This hypothesis is strongly supported by experiments as well as multi-chain simulations. References are given in the following subsections, where a few important results are discussed. Nevertheless, single-chain mean-field entanglement models have struggled with some fundamental issues. A well-known problem is that, in most of these models, the entanglement spacing is not consistent simultaneously with experiments and with multi-chain simulations (see Sec. IC). This consistency is one of four criteria for single-chain mean-field entanglement models, which were considered in a previous publication [5] and are discussed here in Sec. ID. To our knowledge, the only model that satisfies all of them is the anisotropic mobile slip-link model (AMSM) proposed by Schieber *et al.* [5].

* Current address: Dow Benelux BV, Herbert H. Dowweg 5, 4542 NM Hoek; PO box 48, 4530 AA Terneuzen, the Netherlands.

† Current address: Department of Chemical Engineering, Massachusetts Institute of Technology, 77 Massachusetts Avenue, Cambridge, MA 02139, USA

‡ Email: schieber@iit.edu

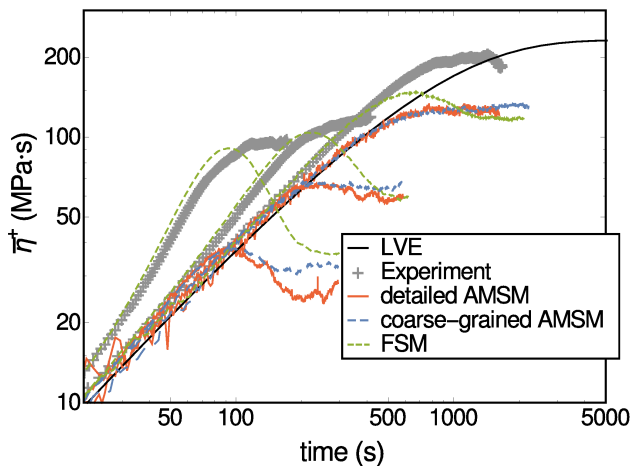


FIG. 1. (Color online) Comparison of slip-link model predictions to uniaxial extension data on a polystyrene melt with $M_w = 200$ kg/mol and $M_w/M_n = 1.04$ [20]. Strain rates $\dot{\epsilon} = 0.003, 0.01,$ and 0.03 s $^{-1}$ (from right to left) were applied at $T = 130$ °C. The FSM assumes affine entanglement motion. The AMSM assumes nonaffine entanglement motion according to the generalized Ronca-Allegra dynamics; see Sec. II C. The detailed AMSM tracks the slip-link positions explicitly, whereas the coarse-grained AMSM tracks only their mean positions [5].

Section II reviews the AMSM and its predecessors from the perspective of these four criteria.

It has been shown in previous publications that the slip-link models by Schieber and co-workers, even those that do not satisfy all four criteria, are in excellent agreement with a wide range of experiments [6–17]. However, some experiments still pose a challenge for entanglement theories in general. Examples are dielectric relaxation in bidisperse blends with a low concentration of high-molecular weight chains [8] and extensional flows [10]. The AMSM does not solve these problems, but it does provide a connection with multi-chain simulations, which enables all of its four parameters to be determined *ab initio*. The molar mass of a Kuhn step, M_K , can be derived from the mean squared end-to-end distance in equilibrated multi-chain systems of sufficiently high molecular weight. The parameters n , related to ESFs, and β , related to the entanglement spacing, can be extracted from primitive-path analysis of such systems [18]. The most convenient way to determine the final parameter, the characteristic time scale τ_K , *ab initio* is by matching the mean squared chain center-of-mass displacement, obtained from molecular dynamics [19]. All of these methods require only equilibrium simulations, which means that the anisotropy of ESFs plays no role. Moreover, the values of these parameters can be mapped onto reduced sets of parameters in each of the less detailed slip-link models [13, 19].

Although the focus of this paper is on compliance with fundamental principles, model predictions are compared

with uniaxial extension data [20] in Fig. 1, from which it is clear that the AMSM performs no better than our earlier fixed slip-link model (FSM) [10]. The FSM captures part of the strain-hardening behavior, but this is followed by a large drop in the extensional viscosity, which is not observed experimentally. The AMSM predictions do not have this severe strain-softening feature, but they also exhibit no significant strain hardening.

Sections I and II provide the context for the main part of the present work: a rigorous proof of consistency with nonequilibrium thermodynamics (one of the four criteria) of the AMSM. This proof, presented in Sec. III, involves demonstrating that the time evolution of the state variables can be written in the form of the general equation for the nonequilibrium reversible-irreversible coupling (GENERIC), which guarantees compliance with the known laws and theorems of nonequilibrium thermodynamics [21–25]. The GENERIC formalism is arguably the most successful theoretical framework for nonequilibrium thermodynamics; the literature contains many examples of its applicability to classical (including relativistic) and quantum-mechanical systems. Detailed comparisons with other nonequilibrium thermodynamics formalisms have also been made [25–35]. The implications of our GENERIC check for the AMSM are summarized, and opportunities for future work are indicated in Sec. IV.

A. Scaling analysis of the entanglement spacing

The most basic characteristic of the entanglement network (or PP network) is the average molecular weight between adjacent entanglements, which is denoted by M_e for a polymer at equilibrium. A few researchers developed simple theories that relate M_e to chain dimensions for linear flexible polymers. Independently of each other, Lin [36] and Kavassalis and Noolandi [37, 38, 39] postulated that the number of entanglement strands inside the volume spanned by one entanglement strand of average length is a universal topological parameter, independent of the chemical structure of the polymer. Lin [36] derived a relation between this parameter and M_e , which is given in Eq. (1) below. Kavassalis and Noolandi’s derivation is analogous to Lin’s, except that they accounted for the presence of dangling ends in addition to entanglement strands. In the long-chain limit, their result reduces to that of Lin [39]. Polydispersity only modifies the dangling-end correction [38].

The volume physically occupied by an entanglement strand of average length is $V_e = M_e/(\rho N_A)$, while a reasonable scaling relation for the volume spanned by such a strand is $V_{e,sp} \propto (M_e \langle R_{ee}^2 \rangle_{eq} / M)^{3/2}$. Here M is the molecular weight of the chain, R_{ee} is its end-to-end distance, and $\langle \dots \rangle_{eq}$ denotes the equilibrium average. Disregarding dangling ends, the number of entanglement strands inside the volume spanned by one entanglement

strand of average length is then

$$\frac{V_{e,sp}}{V_e} \propto \rho N_A \sqrt{M_e} \left(\frac{\langle R_{ee}^2 \rangle_{eq}}{M} \right)^{3/2}. \quad (1)$$

Note that this is a scaling relation, not an equality as suggested by the works of Lin [36] and Kavassalis and Noolandi [37, 38, 39], because the relation between $V_{e,sp}$ and $\langle R_{ee}^2 \rangle_{eq}$ contains an unknown prefactor. Kavassalis and Noolandi [39] recognized that this prefactor depends on the assumed shape of the spanned volume. More importantly, however, it is very sensitive to the characteristic size of this volume. For example, if we take the root-mean-square radius of gyration of the entanglement strand instead of its root-mean-square end-to-end distance, the prefactor is multiplied by $6^{-3/2} \approx 6.8 \times 10^{-2}$. Thus Eq. (1) cannot be used to quantify the number of entanglement strands inside the volume spanned by one entanglement strand. On a side note, attempts at such quantification are also complicated by the fact that M_e cannot be measured directly. It is usually inferred from the plateau modulus, which introduces an additional model-dependent prefactor, as discussed in Sec. IB and in more detail in Ref. [18].

The important result of the Lin-Kavassalis-Noolandi analysis is that the right-hand side of Eq. (1) was found to be constant, within experimental uncertainty, for several different polymers [36, 39]. If the topological parameter $V_{e,sp}/V_e$ is absorbed in the unknown prefactor, Eq. (1) can be written in the form

$$\frac{M_e}{\rho N_A} \propto p^3 = \left(\frac{M}{\rho N_A \langle R_{ee}^2 \rangle_{eq}} \right)^3 \quad (2)$$

as presented by Fetters *et al.* [40], where the packing length p is defined as the volume of the chain divided by its mean squared end-to-end distance. The packing length can also be written in a way that it is proportional to the ‘‘cross-sectional area’’ of a Kuhn step divided by its length, hence p may be interpreted as a measure of chain ‘‘fatness’’ [41]. The relation between M_e and the plateau modulus G_N^0 , as predicted by entanglement models, is generally of the form

$$M_e \propto \frac{\rho RT}{G_N^0}. \quad (3)$$

For a wide variety of nearly monodisperse polymers, Fetters and co-workers [40–44] tabulated the ratio $\langle R_{ee}^2 \rangle_{eq}/M$, obtained from small-angle neutron scattering data, and G_N^0 , obtained from rheological measurements. Consistent with the works of Lin [36] and Kavassalis and Noolandi [37, 38, 39], the results of Fetters and co-workers invariably confirmed the validity of Eq. (2), which is therefore considered a universal scaling relation for entangled polymers.

B. Entanglement spacing from the plateau modulus

Since there is no way to measure M_e directly, it would be convenient if one could calculate it from measurable quantities. Starting from the Lin-Kavassalis-Noolandi postulate, such a calculation is not feasible because it involves unknown prefactors, related to the volume spanned by an entanglement strand and the critical number of other entanglement strands in that volume. A more promising starting point is the relation between the entanglement molecular weight and the plateau modulus, Eq. (3). However, the value of the prefactor in this relation varies significantly between models. It equals 1 in some tube models, but 4/5 in others [45–47]. The slip-link models of Schieber and co-workers predict expressions for the plateau modulus that are weakly dependent on the molecular weight. In the long-chain limit, $M/M_e \rightarrow \infty$, these expressions are consistent with Eq. (3) with a prefactor of 1 [6, 48], except when the spatial positions of the slip-links are allowed to fluctuate by placing them in confinement potentials *and* these potentials become anisotropic in flow. If the anisotropy is described by a lower-convected second-order tensor for each confinement potential, then the prefactor in Eq. (3) decreases as the overall confinement strength decreases, or as the size of the fluctuations, which we call entanglement spatial fluctuations (ESFs), increases [5].

C. Primitive-path analysis

In the early 21st century, algorithms were developed to extract the PP network from atomistic (or nearly atomistic) multi-chain simulations [49–54]. These algorithms shrink all chains in a simulation box simultaneously, under the constraint that they cannot pass through each other, while their ends are kept fixed in space. Eventually, all chains are pulled taut between topological constraints, and a system of entangled, piecewise linear space curves remains. Several research groups have attempted to map this PP network onto a single-chain model, with the objective to extract parameter values from first principles for rheology predictions. In the majority of studies, the Doi-Edwards tube model [45, 55–58] was used, and the parameter M_e was determined through a mapping involving the average PP length at equilibrium. While the result agreed with the value of M_e estimated from the plateau modulus, the actual mesh size of the multi-chain PP network was consistently found to be smaller, roughly by a factor of 2 [51, 53, 59–65].

This difference may be partly explained by the fact that, when PP analysis is applied to a snapshot of a multi-chain simulation, many of the instantaneous topological constraints are too short-lived to affect the stress, which means that they should not be considered as entanglements [4]. The mesh size of the real PP network (i.e., the entanglement network) is thus greater than that of the apparent PP network in a snapshot, and closer to

the estimate of M_e based on the plateau modulus. According to Anogiannakis *et al.* [4], short-lived topological constraints originate from contacts between PPs due to small displacements of the entanglements, which do not significantly change the PP conformations. Estimates of M_e based on the PP-length distribution are therefore insensitive to the presence of these constraints. However, the estimates used in mapping equilibrium PP statistics onto the Doi-Edwards model, which are based on the average PP length at equilibrium [64], involve a number of assumptions that influence the results significantly [18].

More recently, dynamic methods emerged as alternatives to the usual static PP analysis. One group extracted the time evolution of PP conformations from molecular-dynamics simulations and mapped this onto the “segment survival probability function” of tube models [66–70]. Others focused on developing new ways to obtain the PP network from molecular-dynamics trajectories, based on time- and ensemble-averaging [71, 72] or a criterion to select the most persistent topological constraints [4], or a combination of these two approaches [73]. However, Uchida *et al.* [74] showed that the mesh size of PP networks is related to the packing length, which is a purely static property. This is a strong indication that it should be possible to map multi-chain simulations onto a single-chain model using only equilibrium PP statistics. Also, being a static quantity, the PP can be considered as a thermodynamic object.

Tube models disregard many fluctuations that exist in multi-chain simulations, such as fluctuations in the number of entanglements per chain, the number of monomers per strand, and the end-to-end length of each strand. The slip-link model of Schieber [75] does include fluctuations in these variables and gives analytic results for their distributions at equilibrium. Multi-chain simulations have provided quantitative validation of some of these results: the Poisson distribution of the number of entanglements per chain [59] and (except for very short strands) the exponential distribution of the number of monomers per strand [53]. When ESFs are included [48], the equilibrium PP-length distribution from multi-chain systems can be fitted almost perfectly by adjusting the model parameters n , which determines the size of ESFs, and β , which determines the entanglement molecular weight [18]. The resulting value of β is lower than what was found for the slip-link model without ESFs, by fitting either the average PP length at equilibrium from multi-chain simulations [76] or the dynamic modulus from experiments [6, 10]. Thus the entanglement molecular weight becomes lower with ESFs. Most importantly, Steenbakkers *et al.* [18] showed that the short-time relaxation modulus, predicted by PP analysis using the AMSM, agreed well with experimental plateau modulus data for the three chemistries that they tested.

D. Consistency criteria for entanglement models

Simultaneous agreement of the slip-link model with multi-chain simulations and experimental rheology data is achieved only if the ESFs become anisotropic in flow, according to a lower-convected evolution of the entanglement confinement potentials [5, 18]. This anisotropy is intimately related to more fundamental issues of consistency. Schieber *et al.* [5] evaluated a number of single-chain mean-field entanglement models with respect to the following criteria:

- (i) *Consistency with multi-chain models and simulations.* As explained in Sec. IC, the amount of information about multi-chain conformational statistics, which is retained on the single-chain level of description, differs among entanglement models. They all predict a plateau modulus, which depends on a parameter associated with the entanglement molecular weight, so for each model it can be checked whether these two quantities agree simultaneously with multi-chain results. This was the criterion used in our previous work [5]. From the discussion at the end of Sec. IC, it is clear that a more detailed analysis is possible for slip-link models. Here, in addition to the correct prediction of the plateau modulus, we demand that the distributions (not just the averages) of the number of entanglements per chain, the number of monomers per strand, and the PP length are consistent with their counterparts in a multi-chain system at equilibrium.
- (ii) *Consistency with nonequilibrium thermodynamics.* Several theoretical frameworks are available to check whether a model complies with all the laws and theorems of nonequilibrium thermodynamics. The most successful one is the GENERIC formalism, which is used here.
- (iii) *Consistency with the stress-optical rule.* It can be shown analytically that an entanglement strand with end-to-end vector \mathbf{Q} , which contains N Kuhn steps, has a contribution to the refractive index tensor proportional to $\mathbf{Q}\mathbf{Q}/N$ [77]. Experimentally, the extra stress tensor of entangled polymers is found to be proportional to the refractive index tensor, as long as the stress is low enough for the distribution of strand conformations to remain approximately Gaussian [78]. Therefore, under these conditions, the stress tensor must have the form $\boldsymbol{\tau} \sim \langle \sum_{i=1}^Z \mathbf{Q}_i \mathbf{Q}_i / N_i \rangle$, where Z is the number of strands in a chain.
- (iv) *Consistency between the relaxation modulus predicted by the Green-Kubo relation at equilibrium and the modulus after infinitesimal deformation.* The equilibrium relaxation modulus $G(t)$ can be obtained from the stress tensor using the Green-Kubo relation [79]. If the evolution equations of

the conformational variables are known, it is also possible to calculate the stress tensor to linear order in the deformation tensor, and thus obtain the modulus after infinitesimal deformation. According to linear response theory, these two calculations should give the same result.

The models from previous literature, which were considered by Schieber *et al.* [5], all violate at least one of these criteria. This includes the fixed slip-link model (FSM) developed by Schieber and co-workers [6–11], which satisfies criteria (ii)–(iv) but is not in full compliance with criterion (i) [76]. Therefore, we proposed a mobile slip-link model (MSM), which appears to be the first molecular entanglement model to satisfy all four criteria simultaneously [5]. Note that the FSM was originally called the discrete slip-link model (DSM). The latter term is now used to indicate a hierarchy of models, which includes the MSM, the FSM, and another, further coarse-grained model, namely the clustered fixed slip-link model [12–17]. Each of these models is derived by systematic coarse-graining from the next, more detailed member of the hierarchy.

The FSM and the MSM are stochastic models describing the evolution of the PP conformation. The chain resides in a chemical potential bath of activity β , which determines the probability distribution of the number of entanglements at equilibrium [75]. The three dynamic processes that these models have in common are as follows: sliding dynamics (SD) of the chain through the slip-links, creation and destruction of entanglements at the ends of the chain due to SD, and creation and destruction of entanglements anywhere along the chain due to sliding dynamics in its environment. The third process is called constraint dynamics (CD) and is obtained by enforcing consistency with SD [6, 10].

The remaining dynamics are related to entanglement motion, and this is where the two models differ. In the FSM, the slip-links occupy fixed positions relative to the macroscopic deformation, i.e., their motion is affine. In the MSM, the slip-links fluctuate around “anchors” that move affinely. These fluctuations are what we call the ESFs, and they are essential to achieve full compliance with the four criteria. Specifically, the directionality of ESFs needs to follow an upper-convected time evolution (equivalent to lower-convected confinement potentials, as mentioned above). Otherwise at least one criterion is violated [5]. This time evolution is a generalization of the anisotropic dynamics of network node fluctuations in cross-linked network models, first introduced by Ronca and Allegra [80]. Therefore, we refer to it as the generalized Ronca-Allegra dynamics. The slip-link model with generalized Ronca-Allegra dynamics is called the anisotropic mobile slip-link model (AMSM). An older model with isotropic ESFs [48, 81] is called the isotropic mobile slip-link model (IMSM).

Schieber *et al.* [5] compared a number of single-chain mean-field entanglement models from the perspective of the four criteria listed above. However, consistency with

multi-chain simulations was not verified thoroughly. It was merely checked, for each model, whether ESFs are included and whether they lower the plateau modulus, in qualitative agreement with multi-chain simulations of entangled polymer melts [82]. Multi-strand models [83–87] and simulations [82] of cross-linked networks predict a similar effect of network node fluctuations on the elastic modulus. The FSM fails this test because it does not include ESFs. The IMSM fails as well because its plateau modulus is not affected by the ESFs [48]. The AMSM, on the other hand, does predict a plateau modulus that decreases with increasing ESFs. Primitive-path analysis provides a more comprehensive check of consistency with multi-chain simulations, and the results confirm that the AMSM satisfies this criterion, as summarized in Sec. IC and discussed in detail by Steenbakkens *et al.* [18]. Schieber and Andreev [13] and Becerra *et al.* [19] showed that the FSM can accurately reproduce the dynamic modulus of the AMSM by an appropriate rescaling of the parameters. Hence, the FSM represents a faithful coarse-graining of the more fundamental AMSM.

One thing missing from previous work is a rigorous proof that the AMSM is consistent with nonequilibrium thermodynamics. Such a proof is provided here for one of the two versions of the model proposed by Schieber *et al.* [5]. This version exists on a more detailed level of description, which keeps track of the actual slip-link positions, whereas the other has the actual positions of the slip-links coarse-grained out and keeps track only of their mean positions. The proof of thermodynamic consistency is presented in Sec. III for the detailed AMSM. In Sec. II, we review our previous findings related to the compliance of the FSM, the IMSM, and the AMSM with the four criteria [5, 18]. The mobile slip-link models are considered on the detailed level of description here, but all findings carry over to the coarse-grained level of description [5]. The main conclusions are that the AMSM satisfies all four criteria and that this is a direct result of the generalized Ronca-Allegra dynamics, used to describe the flow-induced anisotropy of ESFs. Opportunities for future work on molecular entanglement models are discussed in Sec. IV.

II. ENTANGLEMENT MOTION IN SLIP-LINK MODELS

In all slip-link models considered in this paper, the equilibrium probability density for the chain conformation has the form

$$\begin{aligned}
 p_{\text{eq}}(\Omega) &= \frac{1}{J} \delta_{N_{\mathcal{K}}, \sum_{i=1}^Z N_i} \exp\left(\frac{(Z-1)\mu_e - F(\Omega)}{k_B T}\right) \\
 &= \frac{1}{J \beta^{Z-1}} \delta_{N_{\mathcal{K}}, \sum_{i=1}^Z N_i} \exp\left(-\frac{F(\Omega)}{k_B T}\right). \quad (4)
 \end{aligned}$$

Here Ω is a set of variables including, for each model, the number of entanglement strands Z and the numbers of

Kuhn steps in the strands $\{N_i\}$, which are restricted to integer values. The other variables in Ω , related to the strand conformations and ESFs, are different for each model. The exponential term on the first line of Eq. (4) corresponds to a grand-canonical ensemble with chemical potential μ_e , conjugate to the number of entanglements $Z - 1$, and chain free energy $F(\Omega)$. As in previous work, we use the entanglement activity

$$\beta := \exp\left(-\frac{\mu_e}{k_B T}\right) \quad (5)$$

as a model parameter. The Kronecker δ in Eq. (4) ensures conservation of the total number of Kuhn steps in the chain, N_K . Finally, J is a normalization constant, which can be calculated analytically [48, 75].

The evolution of the probability density $p(\Omega)$ is given by the differential Chapman-Kolmogorov equation,

$$\frac{Dp(\Omega)}{Dt} = \mathcal{L}(\Omega) * p(\Omega) + \int [W(\Omega|\Omega')p(\Omega') - W(\Omega'|\Omega)p(\Omega)] d\Omega', \quad (6)$$

where $\mathcal{L}(\Omega)$ is a linear Fokker-Planck operator describing the dynamics of entanglement motion. In the AMSM, this includes the generalized Ronca-Allegra dynamics. The asterisk represents a general scalar product, which, depending on the operator, may involve differentiation, summation over discrete variables, and integration over continuous variables. The shorthand

$$\frac{D}{Dt} \equiv \frac{\partial}{\partial t} + \mathbf{v} \cdot \nabla \quad (7)$$

denotes the substantial derivative. The second term on the right-hand side of Eq. (6) corresponds to a master equation, which describes the shuffling of Kuhn steps between adjacent strands, i.e., SD, as well as the creation and destruction of entanglements by SD and CD. Here $W(\Omega|\Omega')$ is the transition rate for a jump from conformation Ω' to conformation Ω , and $\int d\Omega'$ is a shorthand that denotes summation over all possible values of the discrete variables and integration over all possible values of the continuous variables.

A. Fixed slip-link model

In the FSM, the chain conformation is expressed in the set of variables

$$\Omega = \{Z, \{N_i, \mathbf{Q}_i\}_{i=1}^Z\}, \quad (8)$$

where

$$\mathbf{Q}_i = \mathbf{R}_i - \mathbf{R}_{i-1} \quad (9)$$

is the end-to-end vector of the i^{th} strand. The vectors $\{\mathbf{R}_i\}$ give the spatial positions of the slip-links

($i \in \{1, 2, \dots, Z-1\}$) and the chain ends ($i \in \{0, Z\}$). By selecting the strand end-to-end vectors as variables, only the relative positions of the slip-links are tracked, and the scope of the model is restricted to problems where center-of-mass diffusion of the chain is unimportant.

The chain free energy F is written as a sum of independent strand free energies F_s ,

$$F(\Omega) = \sum_{i=1}^Z F_s(N_i, \mathbf{Q}_i). \quad (10)$$

Thus we restrict ourselves to flexible polymers. More precisely, we assume that strands with a contour length smaller than the persistence length of the chain have a negligible probability. On the other hand, the form of F_s is not specified here. Finite extensibility can be taken into account by using an approximation to the inverse Langevin function. Cohen's Padé approximant [88] was chosen in our previous work [10], but more accurate alternatives have been derived in recent years [89–91].

The stress tensor can be derived from the response to an instantaneous step strain $\mathbf{E}(t) = \mathbf{E}_0 H(t)$, where $H(t)$ is the Heaviside function. Using the principle of virtual work [92, 93] and integrating over an infinitesimal time interval around the step, we obtain

$$\boldsymbol{\tau} : \mathbf{E}_0 = -n_c \left\langle \int_{F(\Omega; t=0^-)}^{F(\Omega; t=0^+)} dF(\Omega) \right\rangle. \quad (11)$$

Here the angle brackets denote the ensemble average,

$$\langle \dots \rangle \equiv \int \dots p(\Omega) d\Omega, \quad (12)$$

and n_c is the number density of chains. For a monodisperse polymer melt,

$$n_c = \frac{N_A \rho}{M}, \quad (13)$$

where M is the molecular weight and N_A is Avogadro's number. For a monodisperse polymer solution, the right-hand side of Eq. (13) should be multiplied by the polymer weight fraction (if ρ is the density of the solution) or by the polymer volume fraction (if ρ is the density of the polymer). Similarly, for polydisperse systems, the number density of each component of the molecular weight distribution is given by an expression like Eq. (13), multiplied by the appropriate fraction of the component. No modifications to the mathematical structure of the FSM are necessary to account for the presence of solvent [12] or for polydispersity of the polymer, other than a straightforward extension to multiple components in the latter case [7, 11, 17].

In Eq. (11), all dynamics independent of the velocity gradient tensor $\boldsymbol{\kappa}(t) = \mathbf{E}_0 \delta(t)$ vanish identically. Substitution of the affine slip-link motions

$$\frac{d\mathbf{Q}_i}{dt} = \boldsymbol{\kappa} \cdot \mathbf{Q}_i \quad (14)$$

TABLE I. Slip-link models and their consistency with the four criteria from Sec. ID: MC denotes multi-chain models/simulations, NETD denotes nonequilibrium thermodynamics, SOR denotes the stress-optical rule, and GKR denotes the Green-Kubo relation.

Model	Refs.	Criterion			
		(i) MC	(ii) NETD	(iii) SOR	(iv) GKR
FSM	6–11	×	✓	✓	✓
IMSM	48, 81	×	✓	×	✓
AMSM	5, 18	✓	✓	✓	✓

then leads to the stress tensor

$$\boldsymbol{\tau} = -n_c \left\langle \sum_{i=1}^Z \mathbf{Q}_i \frac{\partial F_s}{\partial \mathbf{Q}_i} \right\rangle. \quad (15)$$

Schieber [94] proved that the FSM conforms to the GENERIC structure of nonequilibrium thermodynamics [21–25]. The stress tensor, which follows from the restrictions imposed by the GENERIC structure, is given by Eq. (15) with an additional term proportional to the unit tensor. The prefactor of this term equals $n_c k_B T$ times the average number of variables contributing to the momentum of the system. In the FSM with variables Ω given by Eq. (8), these are the vectors $\{\mathbf{Q}_i\}$, hence the prefactor is $n_c k_B T \langle Z \rangle$. If, instead of $\{\mathbf{Q}_i\}$, we choose the position vectors $\{\mathbf{R}_i\}$ as variables, the prefactor becomes $n_c k_B T (\langle Z \rangle + 1)$. More insight into the origin of the isotropic part of the stress tensor is provided in Sec. III A 1.

Only the conformational part of the stress tensor, Eq. (15), contributes to shear stresses and normal stress differences. It can be shown that this part has the form required by the stress-optical rule [77] by taking

$$\frac{F_s(N_i, \mathbf{Q}_i)}{k_B T} = \frac{3\mathbf{Q}_i^2}{2N_i a_K^2} + \frac{3}{2} \log \left(\frac{2\pi N_i a_K^2}{3} \right), \quad (16)$$

corresponding to a Gaussian strand. (The second term, where log denotes the natural logarithm, is needed to keep the probability density normalized.) The stress-optical rule is then satisfied for all possible strand conformations. With a non-Gaussian free energy, it is satisfied only when the strands are not significantly extended, which is consistent with experimental results [78].

The relaxation modulus $G(t)$ is by definition independent of the isotropic part of the stress tensor. Using the Green-Kubo relation, the initial modulus is found to be [6]

$$G(0) = n_c k_B T \langle Z \rangle_{\text{eq}}. \quad (17)$$

Since $G(t)$ includes longitudinal relaxation modes of the PP, it is somewhat higher than the experimental plateau modulus. Taking the time derivative of Eq. (15) and substituting Eq. (14), the modulus after infinitesimal deformation is found to be equivalent to $G(0)$ from the Green-Kubo relation. Thus the FSM satisfies criteria (ii)-(iv).

This is indicated by check marks in the corresponding columns of Table I.

From the equilibrium probability density $p_{\text{eq}}(\Omega)$, analytic expressions are obtained for the distributions of all variables at equilibrium [75]. The distributions of the number of entanglements per chain $p_{\text{eq}}(Z)$ and the number of Kuhn steps per strand $p_{\text{eq}}(N)$ agree very well with results from multi-chain simulations [53, 59]. Only very short strands deviate from the slip-link prediction for $p_{\text{eq}}(N)$, which can be fixed by including a repulsion between adjacent entanglements on the chain [53]. Also, the molecular-weight dependence of the average PP length at equilibrium is reproduced, but the PP-length distribution is broader than that extracted from multi-chain simulations [76]. Therefore, although the FSM captures much of the physics of multi-chain systems, we conclude that it still violates criterion (i), and put a cross in the corresponding column of Table I.

B. Isotropic mobile slip-link model

Since polymer chains are fluctuating objects, ESFs almost certainly occur in reality. They have indeed been observed in multi-chain simulations [4], hence including them on a single-chain level of description seems a reasonable approach to fixing the violation of criterion (i). In the slip-spring simulation of Likhtman [95] and in the IMSM [48], ESFs are modeled by placing each slip-link in an isotropic confinement potential. This is symbolized by virtual springs, connecting each slip-link to a fixed anchor as in Fig. 2. The centers of the confinement potentials, or anchors of the virtual springs, are assumed to move affinely.

In the IMSM, the conformation of the chain is described by the variables

$$\Omega = \{Z, \{N_i, \mathbf{Q}_i\}_{i=1}^Z, \{\mathbf{X}_i\}_{i=1}^{Z-1}\}, \quad (18)$$

where

$$\mathbf{X}_i = \mathbf{R}_i - \mathbf{r}_i \quad (19)$$

is the vector pointing from the i^{th} anchor to the i^{th} slip-link. Figure 2 illustrates how the vectorial quantities are defined.

The confinement potentials are assumed to be quadratic and isotropic. The chain free energy is then

$$F(\Omega) = \sum_{i=1}^Z F_s(N_i, \mathbf{Q}_i) + \frac{3k_B T}{2na_K^2} \sum_{i=1}^{Z-1} \mathbf{X}_i^2. \quad (20)$$

The parameter n determines the size of ESFs: the higher n is, the softer are the confinement potentials and the larger are the ESFs. Because ESFs contribute to the chain free energy, thermodynamics demands that they also contribute to the stress tensor. This can be shown by means of a virtual-work argument as in Sec. II A. The strands and the virtual springs no longer deform affinely,

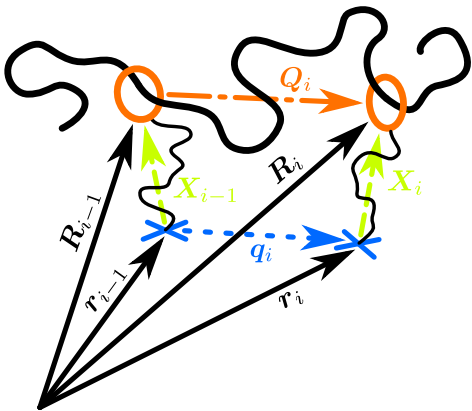


FIG. 2. (Color online) Sketch of a strand on the detailed MSM level of description. The chain (thick black line) passes through slip-links (orange circles) connected to affinely moving anchors (blue crosses) by virtual springs (thin black lines). The black solid arrows are the position vectors of the slip-links and anchors that make up two adjacent entanglements. The orange dash-dotted arrow is the strand end-to-end vector. The green dashed arrows are the virtual-spring end-to-end vectors. The blue dotted arrow is the anchor connector vector.

but the nonaffine contributions to their dynamics vanish identically when integrating over an infinitesimal time interval. Consequently, Eq. (11) yields

$$\tau = -n_c \left\langle \sum_{i=1}^Z \mathbf{Q}_i \frac{\partial F_s}{\partial \mathbf{Q}_i} + \frac{3k_B T}{na_K^2} \sum_{i=1}^{Z-1} \mathbf{X}_i \mathbf{X}_i \right\rangle. \quad (21)$$

Again, the GENERIC result has an additional isotropic term, whose prefactor equals $n_c k_B T$ times the average number of variables contributing to the momentum of the system. In the IMSM, these variables are the vectors $\{\mathbf{Q}_i, \mathbf{X}_i\}$, hence the prefactor is $n_c k_B T(2\langle Z \rangle - 1)$.

Likhtman [95] decided to omit the part due to ESFs from the stress tensor expression, which is then consistent with the stress-optical rule [77]. However, recent work on associating polymers suggests that this leads to a violation of the second law of thermodynamics [96]. An inconsistency in the slip-spring simulation between Green-Kubo predictions and the modulus after infinitesimal deformation was resolved by Ramírez *et al.* [97], but they did not change the definition of the stress tensor, and therefore the thermodynamic issue remains.

In the IMSM, the stress due to the confinement potentials, the second term in Eq. (21), is not omitted. As a result, the model is thermodynamically consistent but violates the stress-optical rule. It is not fully consistent with multi-chain simulations either, since it predicts the same initial relaxation modulus as the FSM, given by Eq. (17) [48], whereas multi-chain simulations show that the plateau modulus decreases with increasing ESFs [82].

The IMSM does yield a modulus after infinitesimal deformation that is consistent with the Green-Kubo relation, hence it satisfies two of the four criteria: one fewer than the FSM. These findings are summarized in Table I.

On the bright side, we found that the equilibrium distribution of the mean-path length, predicted by the IMSM, is practically identical to that obtained from PP analysis of multi-chain systems [18]. The mean path is defined as the shortest path between the chain ends, passing through the mean positions of the slip-links, i.e., those positions that minimize the chain free energy for given anchor positions and given numbers of Kuhn steps in the strands [81]. An important result is that the parameters n and β , obtained by fitting the mean-path length distribution to the multi-chain PP length distribution, are independent of molecular weight, as expected [18]. Thus the discrepancy in PP statistics between the FSM and multi-chain simulations [76] is overcome by the presence of ESFs in the IMSM. Moreover, it can be shown analytically that the mean strand end-to-end vectors are correlated with their neighbors [5, 18, 81], which suggests that the IMSM explains the exponentially decaying correlations between PP segments, observed in multi-chain simulations by Tzoumanekas and Theodorou [53]. We are not aware of similar agreement elsewhere in the literature.

C. Anisotropic mobile slip-link model

The generalized Ronca-Allegra dynamics are the missing ingredient, necessary to satisfy all four consistency criteria simultaneously. In the AMSM, these dynamics are taken into account by a set of shape tensors $\{\mathbf{n}_i\}$, which describe the strength and the directionality of ESFs. We choose the variables

$$\Omega = \{Z, \{N_i, \mathbf{Q}_i\}_{i=1}^Z, \{\mathbf{X}_i, \mathbf{n}_i\}_{i=1}^{Z-1}\}. \quad (22)$$

The chain free energy is then

$$F(\Omega) = \sum_{i=1}^Z F_s(N_i, \mathbf{Q}_i) + \frac{3k_B T}{2a_K^2} \sum_{i=1}^{Z-1} \mathbf{X}_i \cdot \mathbf{n}_i^{-1} \cdot \mathbf{X}_i, \quad (23)$$

again assuming that the confinement potentials are quadratic. At equilibrium, the shape tensors are isotropic ($\mathbf{n}_{i,\text{eq}} = n\delta$) and hence all equilibrium statistics are the same as in the IMSM. Each newly created entanglement also has an isotropic shape tensor. As a result, when flow stops, the isotropy of ESFs is restored by creation and destruction dynamics.

The stress tensor is again found by applying a step strain and using the principle of virtual work. From Eq. (11),

$$\boldsymbol{\tau} : \mathbf{E}_0 = -n_c \left\langle \sum_{i=1}^Z \mathbf{Q}_i \frac{\partial F_s}{\partial \mathbf{Q}_i} + \frac{3k_{\text{BT}}}{2a_{\text{K}}^2} \sum_{i=1}^{Z-1} \mathbf{X}_i \cdot \left(\int_{\mathbf{n}_i^{-1}(t=0^-)}^{\mathbf{n}_i^{-1}(t=0^+)} d\mathbf{n}_i^{-1} + \mathbf{E}_0^\dagger \cdot \mathbf{n}_i^{-1} + \mathbf{n}_i^{-1} \cdot \mathbf{E}_0 \right) \cdot \mathbf{X}_i \right\rangle. \quad (24)$$

This shows that a lower-convected evolution of the confinement potentials,

$$\frac{d\mathbf{n}_i^{-1}}{dt} = -\boldsymbol{\kappa}^\dagger \cdot \mathbf{n}_i^{-1} - \mathbf{n}_i^{-1} \cdot \boldsymbol{\kappa}, \quad (25)$$

or, equivalently, an upper-convected evolution of the shape tensors,

$$\frac{d\mathbf{n}_i}{dt} = \boldsymbol{\kappa} \cdot \mathbf{n}_i + \mathbf{n}_i \cdot \boldsymbol{\kappa}^\dagger, \quad (26)$$

leads to the stress tensor

$$\boldsymbol{\tau} = -n_c \left\langle \sum_{i=1}^Z \mathbf{Q}_i \frac{\partial F_s}{\partial \mathbf{Q}_i} \right\rangle. \quad (27)$$

This is identical to Eq. (15) for the FSM, and it agrees with the stress-optical rule. Again, the GENERIC result for the stress tensor includes an isotropic term, related to the number of variables that contribute to the momentum of the system. This term is derived in Sec. III A 1.

The cancellation of ESF terms in the stress tensor also affects the relaxation modulus, which can be calculated by the Green-Kubo relation. At times that are long relative to the relaxation of ESFs, but are on the order of the shortest time scales accessible in rheological measurements, the relaxation modulus should correspond to the experimental plateau modulus. On this intermediate time scale, the relaxation modulus decreases with increasing ESFs [5], which is consistent with multi-chain simulation results [82]. The modulus after infinitesimal deformation remains consistent with $G(0)$ from the Green-Kubo relation [5]. More generally, recent work by Indei [98] suggests that $G(t)$ for a system under small deformation is consistent with the Green-Kubo relation. Since the AMSM has the same equilibrium statistics as the IMSM, the agreement between the equilibrium distribution of the mean-path length and that of the multi-chain PP length is preserved [18]. In summary, all four criteria are satisfied, as indicated in Table I.

The upper-convected evolution of the shape tensors, Eq. (26), is what we call the generalized Ronca-Allegra dynamics, after the network node dynamics introduced by Ronca and Allegra [80] in their model for cross-linked networks. They hypothesized that spatial fluctuations of the cross-links would become anisotropic in flow due to excluded-volume interactions. These interactions were also called “entanglements.” Although the word is the same, the meaning is very different from the topological constraints introduced previously [1–3], which polymer scientists refer to when they talk about entanglements today. Starting from the phantom network model, in which the only interactions are entropic forces exerted by the

network strands on the cross-links, Ronca and Allegra [80] added the hypothetical excluded-volume effects by placing the cross-links in confinement potentials, which are described by a single anisotropic tensor because all cross-links are permanent and present from the outset. Assuming that the anisotropy is not subject to any relaxation process, the principal directions of this tensor coincide with the principal strain directions. Therefore, Ronca and Allegra and later authors [99–102] aligned the coordinate system with the principal strain directions, and then they made each principal component of the confinement potential a function of the corresponding principal strain.

This approach still works for cross-linked networks with trapped entanglements (topological constraints, not excluded-volume interactions) whose ESFs become anisotropic in flow. A trapped entanglement involves at least two chains that lead to a cross-link in either direction; they are called active network chains in the literature. Consequently, the entanglement is not subject to creation and destruction dynamics, and the principal directions of its confinement potential coincide with the principal strain directions. On the other hand, if an entanglement is made up of at most one active network chain, while the other chains have one free end (dangling chains) or two free ends (solvent chains), then the entanglement is subject to creation and destruction dynamics and the principal directions of its confinement potential are generally different from those of the other confinement potentials, as well as from the principal strain directions. As a result, for an entangled melt or a cross-linked network containing entangled dangling chains or solvent chains, there is not one coordinate system in which all confinement potentials are described by diagonal tensors, unless the flow has no shear components. The generalized Ronca-Allegra dynamics are applicable to systems containing arbitrary combinations of cross-links, trapped entanglements, and temporary entanglements, subjected to any kind of flow.

To end this section, we mention a few works in which direct observations of node fluctuations in multi-strand cross-linked network simulations were compared with the Ronca-Allegra dynamics. Allegra *et al.* [103] studied spatial fluctuations in coarse-grained bead-spring simulations of regular hexafunctional polyethylene networks. Applying uniaxial deformation, they looked at correlations between the fluctuations of pairs of network nodes, and they found that these were close to the predictions of the Ronca-Allegra model. Similar results were reported in earlier studies [104, 105], comparing simulations of three-strand micronetworks with a model developed by Flory [106], which is also based on the Ronca-Allegra dynamics.

III. THERMODYNAMIC CONSISTENCY OF THE DETAILED AMSM

To perform the GENERIC check of thermodynamic consistency for the AMSM with variables Ω as in Eq. (22), we need to formulate the nonaffine dynamics of the strand and virtual-spring end-to-end vectors. These can be derived from the equations of motion of the slip-links and anchors. Therefore, we start with the variable set

$$\Omega^+ = \{Z, \{N_i\}_{i=1}^Z, \{\mathbf{R}_i\}_{i=0}^Z, \{\mathbf{r}_i, \mathbf{n}_i\}_{i=1}^{Z-1}\}. \quad (28)$$

On this slightly more detailed level of description, the chain free energy is

$$F(\Omega^+) = \sum_{i=1}^Z F_s(N_i, \mathbf{R}_i - \mathbf{R}_{i-1}) + \frac{3k_B T}{2a_K^2} \sum_{i=1}^{Z-1} (\mathbf{R}_i - \mathbf{r}_i) \cdot \mathbf{n}_i^{-1} \cdot (\mathbf{R}_i - \mathbf{r}_i), \quad (29)$$

equivalent to Eq. (23).

The anchors are assumed to move affinely,

$$\frac{d\mathbf{r}_i}{dt} = \boldsymbol{\kappa} \cdot \mathbf{r}_i dt, \quad (30)$$

and the motion of a chain end or entanglement is given by the Langevin equation

$$d\mathbf{R}_i = \left(\boldsymbol{\kappa} \cdot \mathbf{R}_i - \frac{1}{\zeta} \frac{\partial F(\Omega^+)}{\partial \mathbf{R}_i} \right) dt + \sqrt{\frac{2k_B T}{\zeta}} d\mathbf{W}_i, \quad (31)$$

where $d\mathbf{W}_i$ is a vector of three independent Wiener processes [107] and ζ is a friction coefficient. The term involving $\boldsymbol{\kappa}$ is necessary to recover purely affine motion in the elastic limit, $\zeta \rightarrow \infty$.

As usual, a partial derivative with respect to a certain variable implies that all other variables are kept fixed.

According to Eqs. (9), (19), (22), and (28), partial derivatives of the free energies with respect to the positions or end-to-end vectors are then related by

$$\frac{\partial F(\Omega^+)}{\partial \mathbf{R}_i} = \frac{\partial F(\Omega)}{\partial \mathbf{Q}_i} - \frac{\partial F(\Omega)}{\partial \mathbf{Q}_{i+1}} + \frac{\partial F(\Omega)}{\partial \mathbf{X}_i}. \quad (32)$$

The equations of motion for the strands and virtual springs are derived from Eqs. (9), (19), (30), (31), and (32). The results are

$$d\mathbf{Q}_i = \left(\boldsymbol{\kappa} \cdot \mathbf{Q}_i - \sum_{j=1}^Z \frac{A_{ij}}{\zeta} \frac{\partial F(\Omega)}{\partial \mathbf{Q}_j} - \sum_{j=1}^{Z-1} \frac{B_{ij}}{\zeta} \frac{\partial F(\Omega)}{\partial \mathbf{X}_j} \right) dt + \sqrt{\frac{2k_B T}{\zeta}} \sum_{j=0}^Z B_{ij} d\mathbf{W}_j \quad (33)$$

and

$$d\mathbf{X}_i = \left(\boldsymbol{\kappa} \cdot \mathbf{X}_i - \sum_{j=1}^Z \frac{B_{ji}}{\zeta} \frac{\partial F(\Omega)}{\partial \mathbf{Q}_j} - \frac{1}{\zeta} \frac{\partial F(\Omega)}{\partial \mathbf{X}_i} \right) dt + \sqrt{\frac{2k_B T}{\zeta}} d\mathbf{W}_i, \quad (34)$$

with

$$A_{ij} = -\delta_{i-1,j} + 2\delta_{ij} - \delta_{i+1,j} \quad (35)$$

and

$$B_{ij} = -\delta_{i-1,j} + \delta_{ij}. \quad (36)$$

Using Itô calculus [107], the stochastic differential equations (26), (33), and (34) are rewritten as a Fokker-Planck equation for the probability density. For the corresponding Fokker-Planck part of Eq. (6), we then obtain

$$\begin{aligned} \frac{\mathcal{L}(\Omega) * p(\Omega)}{k_B T} = & - \sum_{i=1}^Z \frac{\partial}{\partial \mathbf{Q}_i} \cdot \left[\boldsymbol{\kappa} \cdot \mathbf{Q}_i \frac{p(\Omega)}{k_B T} - \sum_{j=1}^Z \frac{A_{ij}}{\zeta} \left(\frac{p(\Omega)}{k_B T} \frac{\partial F(\Omega)}{\partial \mathbf{Q}_j} + \frac{\partial p(\Omega)}{\partial \mathbf{Q}_j} \right) - \sum_{j=1}^{Z-1} \frac{B_{ij}}{\zeta} \left(\frac{p(\Omega)}{k_B T} \frac{\partial F(\Omega)}{\partial \mathbf{X}_j} + \frac{\partial p(\Omega)}{\partial \mathbf{X}_j} \right) \right] \\ & - \sum_{i=1}^{Z-1} \frac{\partial}{\partial \mathbf{X}_i} \cdot \left[\boldsymbol{\kappa} \cdot \mathbf{X}_i \frac{p(\Omega)}{k_B T} - \sum_{j=1}^Z \frac{B_{ji}}{\zeta} \left(\frac{p(\Omega)}{k_B T} \frac{\partial F(\Omega)}{\partial \mathbf{Q}_j} + \frac{\partial p(\Omega)}{\partial \mathbf{Q}_j} \right) - \frac{1}{\zeta} \left(\frac{p(\Omega)}{k_B T} \frac{\partial F(\Omega)}{\partial \mathbf{X}_i} + \frac{\partial p(\Omega)}{\partial \mathbf{X}_i} \right) \right] \\ & - \sum_{i=1}^{Z-1} \frac{\partial}{\partial \mathbf{n}_i} : \left[(\boldsymbol{\kappa} \cdot \mathbf{n}_i + \mathbf{n}_i \cdot \boldsymbol{\kappa}^\dagger) \frac{p(\Omega)}{k_B T} \right]. \end{aligned} \quad (37)$$

For an explicit formulation of the master-equation part of Eq. (6), we refer to the literature [6, 10].

A. GENERIC formulation

According to the two-generator formalism of nonequilibrium thermodynamics [21–25], the time evolution of a

closed system is given by

$$\frac{d\mathbf{x}}{dt} = \mathbf{L} * \frac{\delta E}{\delta \mathbf{x}} + \mathbf{M} * \frac{\delta S}{\delta \mathbf{x}}, \quad (38)$$

where \mathbf{x} is a column containing the state variables, chosen to describe the system. This expression is known as the general equation for the nonequilibrium reversible-irreversible coupling, or GENERIC. The reversible part of the dynamics is generated by the operator \mathbf{L} , called the Poisson matrix, acting on the functional derivative of the total energy E of the system with respect to \mathbf{x} . The dissipative part of the dynamics is generated by the operator \mathbf{M} , called the friction matrix, acting on the functional derivative of the total entropy S of the system with respect to \mathbf{x} . This two-generator formalism imposes a number of restrictions on the operators \mathbf{L} and \mathbf{M} . Each must satisfy a degeneracy condition:

$$\mathbf{L} * \frac{\delta S}{\delta \mathbf{x}} = 0, \quad (39)$$

which means that the entropy is not affected by the reversible dynamics, and

$$\mathbf{M} * \frac{\delta E}{\delta \mathbf{x}} = 0, \quad (40)$$

which means that the energy is not affected by the dissipative dynamics. Moreover, \mathbf{L} must be antisymmetric and must satisfy the Jacobi identity, while \mathbf{M} must be symmetric and positive-semidefinite [22–25].

For the AMSM, we choose the state variables

$$\mathbf{x} = \begin{pmatrix} \rho(\mathbf{r}, t) \\ \mathbf{u}(\mathbf{r}, t) \\ \epsilon(\mathbf{r}, t) \\ p(\Omega_a; \mathbf{r}, t) \end{pmatrix}, \quad (41)$$

i.e., the mass density ρ , the momentum density \mathbf{u} , the internal energy density ϵ , and the conformational probability density $p(\Omega_a)$, which all depend on the position \mathbf{r} and time t . The set of variables Ω_a , used to describe the chain conformation, is a slight modification of Ω from Eq. (22). Each shape tensor is decomposed into three symmetric dyads,

$$\mathbf{n}_i = \sum_{\alpha=1}^3 \frac{\mathbf{a}_i^\alpha \mathbf{a}_i^\alpha}{a_K^2}. \quad (42)$$

The division by a_K^2 on the right-hand side is merely for convenience of notation later on. Equation (26) implies the dynamics

$$\frac{d\mathbf{a}_i^\alpha}{dt} = \boldsymbol{\kappa} \cdot \mathbf{a}_i^\alpha, \quad (43)$$

and the condition that the shape tensors are isotropic at equilibrium is satisfied by

$$\mathbf{a}_{i,\text{eq}}^\alpha = \sqrt{n} a_K \boldsymbol{\delta}_\alpha, \quad (44)$$

where $\boldsymbol{\delta}_\alpha$ is the unit vector in the direction of coordinate α . By choosing the vectors $\{\mathbf{a}_i^\alpha\}$ as variables instead of the tensors $\{\mathbf{n}_i\}$, so that

$$\Omega_a = \{Z, \{N_i, \mathbf{Q}_i\}_{i=1}^Z, \{\mathbf{X}_i, \{\mathbf{a}_i^\alpha\}_{\alpha=1}^3}\}_{i=1}^{Z-1}, \quad (45)$$

we can use a result from previous work to show that the Poisson operator satisfies the Jacobi identity. This is explained after Eq. (62). Alternatively, in the variable space Ω , compliance with the Jacobi identity can be proven rigorously using the guidelines given by Öttinger [25] for handling tensors and their derivatives. In terms of the variables Ω_a , the free energy becomes

$$F(\Omega_a) = \sum_{i=1}^Z F_s(N_i, \mathbf{Q}_i) + \frac{3k_B T}{2} \sum_{i=1}^{Z-1} \mathbf{X}_i \cdot \left(\sum_{\alpha=1}^3 \mathbf{a}_i^\alpha \mathbf{a}_i^\alpha \right)^{-1} \cdot \mathbf{X}_i, \quad (46)$$

and the Fokker-Planck part of Eq. (6) becomes

$$\mathcal{L}(\Omega_a) * p(\Omega_a) = \dots - \sum_{i=1}^{Z-1} \sum_{\alpha=1}^3 \frac{\partial}{\partial \mathbf{a}_i^\alpha} \cdot [\boldsymbol{\kappa} \cdot \mathbf{a}_i^\alpha p(\Omega_a)], \quad (47)$$

where the ellipsis represents the terms on the right-hand side of Eq. (37), multiplied by $k_B T$, which are related to the dynamics of the vectors $\{\mathbf{Q}_i, \mathbf{X}_i\}$. After formulating the GENERIC for this model, we can change variables from Ω_a back to Ω .

The position and time dependencies of the state variables are henceforth omitted from our notation. Since the free energy of the chain, given in Eq. (46), is purely entropic, the total energy is

$$E[\rho, \mathbf{u}, \epsilon] = \int \left(\frac{\mathbf{u}^2}{2\rho} + \epsilon \right) d\mathbf{r} \quad (48)$$

as in classical hydrodynamics [23]. The total entropy is

$$S[\rho, \epsilon, p(\Omega_a)] = \int s(\rho, \epsilon) d\mathbf{r} + S_c[\rho, p(\Omega_a)], \quad (49)$$

where $s(\rho, \epsilon)$ is the entropy density related to dynamics that are fast compared to the dynamics of the chain conformation, and

$$S_c[\rho, p(\Omega_a)] = -k_B \iint n_c(\rho) p(\Omega_a) \log \left(\frac{p(\Omega_a)}{p_{\text{eq}}(\Omega_a)} \right) d\Omega_a d\mathbf{r} \quad (50)$$

is the conformational entropy. Although $p_{\text{eq}}(\Omega_a)$, given by Eq. (4), is proportional to a Kronecker δ , there is no problem of division by zero here. Conservation of the number of Kuhn steps in the chain implies that $p(\Omega_a)$ must remain proportional to that Kronecker δ and therefore it cancels out.

Functional derivatives with respect to the mass density and the probability density need to be handled with care.

The usual definition of the functional derivative [108, 109] allows all variations of the argument of the functional, irrespective of any constraints. In the present case, there are two constraints: the integral of the mass density over the volume of the system must remain equal to the total mass of the system,

$$\int \rho(\mathbf{r}) d\mathbf{r} = m, \quad (51)$$

and the probability density must remain normalized,

$$\int p(\Omega_a) d\Omega_a = 1. \quad (52)$$

We compensate for violations of Eq. (51) by making the substitution

$$\rho \rightarrow \frac{m\rho}{\int \rho d\mathbf{r}} \quad (53)$$

before taking functional derivatives with respect to ρ , and for violations of Eq. (52) by making the substitution

$$p(\Omega_a) \rightarrow \frac{p(\Omega_a)}{\int p(\Omega_a) d\Omega_a} \quad (54)$$

before taking functional derivatives with respect to $p(\Omega_a)$. Equations (51) and (52) are used only afterwards to simplify the resulting expressions. Öttinger and Beris [110] introduced this method in their work on a thermodynamically consistent version of the Doi-Edwards tube model without the independent alignment assumption [93]. However, they used it only to preserve normalization of their probability density f for the PP orientation when calculating $\delta S/\delta f$, not to prevent violations of the conservation of mass when calculating $\delta E/\delta \rho$ or $\delta S/\delta \rho$. An alternative approach, presented in Appendix C.3 of Öttinger [25], leads to a slightly different result for the constrained functional derivative. However, that approach involves the choice of an additional constraint to fix an otherwise arbitrary constant. In the Supplemental Material [111], we propose a different choice for this additional constraint, which makes the method of Öttinger [25] equivalent to that of Öttinger and Beris [110].

Under the constraint of mass conservation, the functional derivative of the total energy with respect to the state variables (for short, the energy gradient) becomes

$$\frac{\delta E}{\delta \mathbf{x}} = \begin{pmatrix} -\frac{1}{2}\mathbf{v}^2 + \frac{1}{2m} \int \rho \mathbf{v}^2 d\mathbf{r} \\ \mathbf{v} \\ 1 \\ 0 \end{pmatrix}, \quad (55)$$

where $\mathbf{v} = \mathbf{u}/\rho$ is the velocity. With the definitions of the temperature

$$T := \left(\frac{\partial s(\rho, \epsilon)}{\partial \epsilon} \right)^{-1} \quad (56)$$

and the chemical potential

$$\mu := -T \frac{\partial s(\rho, \epsilon)}{\partial \rho} \quad (57)$$

[23], the resulting entropy gradient is

$$\frac{\delta S}{\delta \mathbf{x}} = \begin{pmatrix} -\frac{\mu}{T} + \frac{1}{m} \int \frac{\rho \mu}{T} d\mathbf{r} + \frac{\delta S_c}{\delta \rho} \\ \mathbf{0} \\ \frac{1}{T} \\ \frac{\delta S_c}{\delta p(\Omega_a)} \end{pmatrix}. \quad (58)$$

The terms involving integrals over space in Eqs. (55) and (58) come from the mass-conservation constraint. The functional derivatives of the conformational entropy are

$$\begin{aligned} \frac{\delta S_c}{\delta \rho} &= -k_B \frac{dn_c}{d\rho} \left[\int p(\Omega_a) \log \left(\frac{p(\Omega_a)}{p_{\text{eq}}(\Omega_a)} \right) d\Omega_a \right. \\ &\quad \left. - \frac{1}{m} \iint \rho p(\Omega_a) \log \left(\frac{p(\Omega_a)}{p_{\text{eq}}(\Omega_a)} \right) d\Omega_a d\mathbf{r} \right], \quad (59) \end{aligned}$$

where the last term is again due to the mass-conservation constraint, and

$$\begin{aligned} \frac{\delta S_c}{\delta p(\Omega_a)} &= -k_B n_c(\rho) \left[\log \left(\frac{p(\Omega_a)}{p_{\text{eq}}(\Omega_a)} \right) \right. \\ &\quad \left. - \int p(\Omega_a) \log \left(\frac{p(\Omega_a)}{p_{\text{eq}}(\Omega_a)} \right) d\Omega_a \right], \quad (60) \end{aligned}$$

where the last term is due to the normalization constraint for $p(\Omega_a)$.

Equations (55), (58), (59), and (60) differ from expressions found in the literature for similar models. In the GENERIC formulation of the Hookean dumbbell model by Öttinger and Grmela [23], functional derivatives with respect to the mass density and the probability density were evaluated without compensating for any constraint violations. The energy and entropy gradients for the thermodynamically consistent tube model, given in Appendix A of Öttinger [112], are missing all terms related to mass conservation because that constraint was not enforced, but they are otherwise equivalent to our Eqs. (55), (58), (59), and (60). Öttinger [25] reported these two models without changing the functional derivatives used in the original publications. This means that the normalization constraint was applied to the tube model in his Sec. 4.3.2, but not to the Hookean dumbbell model in his Sec. 4.3.1, while the mass-conservation constraint was not applied to either model, although it was discussed in his Appendix C.3.

Schieber [94] likewise considered only the normalization constraint, but not the mass-conservation constraint, in the GENERIC formulation of the FSM. Here Schieber's work is corrected and extended to the AMSM, from which the FSM is obtained as a special case without ESFs, and the Hookean dumbbell model is obtained when entanglements are altogether absent. The energy and entropy gradients are primarily used to derive the stress

tensor, as explained in Sec. III A 1. Curiously, the result is the same whether constrained or unconstrained functional derivatives, or even mixtures of them, are used. A formal proof of this is given in Appendix A.

In Appendix B, we present the stress tensor derivation using a probability density that is normalized not to 1, but to the chain number density $n_c(\rho)$. This is consistent with Öttinger and Grmela's choice of state variables for the Hookean dumbbell model [23]. The choice of normalization does not affect the result obtained for the stress tensor. However, we identify an error in the derivation of Öttinger and Grmela, which leads to a different prefactor of the isotropic part of the stress tensor. In Schieber's

work [94], it was not clear how the probability density was normalized. This ambiguity is also resolved in Appendix B.

1. Reversible dynamics

The Poisson matrix for the AMSM is a straightforward generalization of that for the FSM [Eqs. (14) and (15) of Ref. [94]], which in turn is closely related to the Poisson matrix for the Hookean dumbbell model [Eq. (58) of Ref. [23]]. We find

$$\mathbf{L} = - \begin{pmatrix} 0 & \nabla \rho & 0 & 0 \\ \rho \nabla & (\nabla \mathbf{u} + \mathbf{u} \nabla)^\dagger & \epsilon \nabla + \nabla \cdot (P \delta + \mathbf{\Pi}) & -\mathbf{L}_{24} \\ 0 & \nabla \epsilon + (P \delta + \mathbf{\Pi}) \cdot \nabla & 0 & 0 \\ 0 & -\mathbf{L}_{42} & 0 & 0 \end{pmatrix} \quad (61)$$

with P the hydrostatic pressure and $\mathbf{\Pi}$ the stress tensor. According to Eq. (47),

$$-\mathbf{L}_{42} = \nabla p(\Omega_a) - p(\Omega_a) \nabla + \left[\sum_{i=1}^Z \frac{\partial}{\partial \mathbf{Q}_i} p(\Omega_a) \mathbf{Q}_i + \sum_{i=1}^{Z-1} \left(\frac{\partial}{\partial \mathbf{X}_i} p(\Omega_a) \mathbf{X}_i + \sum_{\alpha=1}^3 \frac{\partial}{\partial \mathbf{a}_i^\alpha} p(\Omega_a) \mathbf{a}_i^\alpha \right) \right] \cdot \nabla \quad (62)$$

produces the reversible part of the evolution of $p(\Omega_a)$, which consists of the affine components of the deformation of the strands, the virtual springs, and the vectors $\{\mathbf{a}_i^\alpha\}$. The remaining element \mathbf{L}_{24} is then determined by the antisymmetry and the Jacobian structure of \mathbf{L} . Proving the latter is usually a tedious exercise, but here the change of variables from Ω to Ω_a comes in handy. Equation (62) has almost the same form as the expressions for \mathbf{L}_{42} in the Hookean dumbbell model [Eq. (58) of Ref. [23]] and the FSM [Eq. (14) of Ref. [94]]. In both those expressions, the second term on the right-hand side of Eq. (62) is absent because the probability density was normalized to the chain number density, while it is normalized to 1 here (see Appendix B). The only other differences are in the numbers of vectorial variables: 1 for the Hookean dumbbell model, Z for the FSM, and $5Z - 4$ for the AMSM. Therefore, we can take \mathbf{L}_{24} from Schieber [94] and add the ESFs,

$$-\mathbf{L}_{24} = p(\Omega'_a) \nabla - \nabla p(\Omega'_a) - \nabla \cdot \left[\sum_{i=1}^{Z'} p(\Omega'_a) \mathbf{Q}'_i \frac{\partial}{\partial \mathbf{Q}'_i} + \sum_{i=1}^{Z'-1} p(\Omega'_a) \left(\mathbf{X}'_i \frac{\partial}{\partial \mathbf{X}'_i} + \sum_{\alpha=1}^3 \mathbf{a}'_i^\alpha \frac{\partial}{\partial \mathbf{a}'_i^\alpha} \right) \right], \quad (63)$$

and the Jacobi identity remains fulfilled. The primes indicate that, after multiplication by \mathbf{L}_{24} , the result is summed over all possible values of the discrete variables and integrated over all possible values of the continuous variables in Ω'_a .

The stress tensor $\mathbf{\Pi}$ is completely determined by the degeneracy condition for the Poisson matrix, Eq. (39), and is therefore purely entropic. In general, if the chain free energy has both an entropic and an energetic part, the latter appears in the friction matrix \mathbf{M} to satisfy its degeneracy condition, Eq. (40). This yields a purely energetic contribution to the stress tensor, in addition to $\mathbf{\Pi}$ (see Ref. [23], p. 6644). In the present model, the chain free energy is entropic and therefore $\mathbf{\Pi}$ is the total stress tensor. Since only the second element of $\mathbf{L} * \delta S / \delta \mathbf{x}$ is nontrivially zero, $\mathbf{\Pi}$ is given by

$$\begin{aligned} \mathbf{0} = & \nabla \left(\frac{\mu \rho - \epsilon - P}{k_B T} \right) + \frac{\nabla \epsilon - \mu \nabla \rho}{k_B T} - \nabla \cdot \left(\frac{\mathbf{\Pi}}{k_B T} \right) + n_c(\rho) \nabla \int p(\Omega_a) \log \left(\frac{p(\Omega_a)}{p_{\text{eq}}(\Omega_a)} \right) d\Omega_a \\ & + \int p(\Omega_a) \nabla \left[n_c(\rho) \log \left(\frac{p(\Omega_a)}{p_{\text{eq}}(\Omega_a)} \right) \right] d\Omega_a - \nabla \left[n_c(\rho) \int p(\Omega_a) \log \left(\frac{p(\Omega_a)}{p_{\text{eq}}(\Omega_a)} \right) d\Omega_a \right] \\ & - \nabla \cdot \int n_c(\rho) \left[\sum_{i=1}^Z p(\Omega_a) \mathbf{Q}_i \frac{\partial}{\partial \mathbf{Q}_i} \log \left(\frac{p(\Omega_a)}{p_{\text{eq}}(\Omega_a)} \right) + \sum_{i=1}^{Z-1} p(\Omega_a) \left(\mathbf{X}_i \frac{\partial}{\partial \mathbf{X}_i} + \sum_{\alpha=1}^3 \mathbf{a}_i^\alpha \frac{\partial}{\partial \mathbf{a}_i^\alpha} \right) \log \left(\frac{p(\Omega_a)}{p_{\text{eq}}(\Omega_a)} \right) \right] d\Omega_a. \end{aligned} \quad (64)$$

The first two terms on the right-hand side cancel one another by the fundamental thermodynamic relation

$$d\epsilon = Tds + \mu d\rho \quad (65)$$

and the Gibbs-Duhem relation

$$\epsilon = Ts - P + \mu\rho. \quad (66)$$

The last four terms on the right-hand side of Eq. (64) correspond to the terms on the right-hand side of Eq. (A7), which involve the unconstrained functional derivatives of the conformational entropy with respect to the mass density and the probability density. As shown in Appendix A, the same result is obtained whether constrained or unconstrained functional derivatives are used. The sum of the first three of these terms, divided by $n_c(\rho)$, can be written as

$$\int p(\Omega_a) \nabla \log \left(\frac{p(\Omega_a)}{p_{\text{eq}}(\Omega_a)} \right) d\Omega_a = \left\langle \nabla \left(\frac{F(\Omega_a)}{k_B T} \right) \right\rangle, \quad (67)$$

which simplifies to

$$\int p(\Omega_a) \nabla \log \left(\frac{p(\Omega_a)}{p_{\text{eq}}(\Omega_a)} \right) d\Omega_a = 0 \quad (68)$$

if we assume the chain free energy to be proportional to the temperature, as proposed by Öttinger and Grmela [23] (p. 6641). All remaining terms in Eq. (64) are then of the form $\nabla * (\dots)$, and consequently the stress tensor $\mathbf{\Pi}(\mathbf{r})$, which is derived below, only depends on the local temperature $T(\mathbf{r})$ and the local probability density $p(\Omega_a; \mathbf{r})$. A more general expression for the stress tensor could be obtained by abandoning this assumption and taking the right-hand side of Eq. (67) into account in the derivation below. This approach would lead to a nonlocal stress tensor because $\langle \nabla * (\dots) \rangle \neq \nabla * \langle \dots \rangle$, due to the position dependence of the probability density. However, purely entropic chain free energies (like the ones considered in the present work) usually are proportional to the temperature, so that Eq. (68) holds. According to Öttinger and Grmela [23] (p. 6641), energetic potentials should be incorporated in the energy $E[\mathbf{x}]$ instead of the entropy $S[\mathbf{x}]$. To fulfill the degeneracy requirement for the friction matrix \mathbf{M} , Eq. (40), no assumption needs to be made concerning the form of the energetic potentials [23] (p. 6643).

With Eq. (68), we find for the stress tensor

$$\begin{aligned} \frac{\mathbf{\Pi}}{k_B T} = & -n_c(\rho) \int \left\{ \sum_{i=1}^Z \mathbf{Q}_i \left(\frac{\partial p(\Omega_a)}{\partial \mathbf{Q}_i} + \frac{p(\Omega_a)}{k_B T} \frac{\partial F(\Omega_a)}{\partial \mathbf{Q}_i} \right) \right. \\ & + \sum_{i=1}^{Z-1} \left[\mathbf{X}_i \left(\frac{\partial p(\Omega_a)}{\partial \mathbf{X}_i} + \frac{p(\Omega_a)}{k_B T} \frac{\partial F(\Omega_a)}{\partial \mathbf{X}_i} \right) \right. \\ & \left. \left. + \sum_{\alpha=1}^3 \mathbf{a}_i^\alpha \left(\frac{\partial p(\Omega_a)}{\partial \mathbf{a}_i^\alpha} + \frac{p(\Omega_a)}{k_B T} \frac{\partial F(\Omega_a)}{\partial \mathbf{a}_i^\alpha} \right) \right] \right\} d\Omega_a. \end{aligned} \quad (69)$$

The terms involving derivatives of $p(\Omega_a)$ simplify after integration by parts, using

$$\lim_{Q_i \rightarrow Q_{\text{max}}} p(\Omega_a) = 0, \quad (70)$$

$$\lim_{X_i \rightarrow \infty} p(\Omega_a) = 0, \quad (71)$$

$$\lim_{a_i^\alpha \rightarrow \infty} p(\Omega_a) = 0, \quad (72)$$

with $Q_{\text{max}} = \infty$ for infinitely extensible strands and $Q_{\text{max}} = N_K a_K$ for finitely extensible strands. Furthermore, it can be shown that

$$\begin{aligned} \sum_{\alpha=1}^3 \mathbf{a}_i^\alpha \frac{\partial F(\Omega_a)}{\partial \mathbf{a}_i^\alpha} &= -3k_B T \left(\sum_{\alpha=1}^3 \mathbf{a}_i^\alpha \mathbf{a}_i^\alpha \right)^{-1} \cdot \mathbf{X}_i \mathbf{X}_i \\ &= -\mathbf{X}_i \frac{\partial F(\Omega_a)}{\partial \mathbf{X}_i} \end{aligned} \quad (73)$$

and thus the stress tensor becomes

$$\mathbf{\Pi} = k_B T n_c(\rho) (5\langle Z \rangle - 4) \boldsymbol{\delta} - n_c(\rho) \left\langle \sum_{i=1}^Z \mathbf{Q}_i \frac{\partial F_s}{\partial \mathbf{Q}_i} \right\rangle. \quad (74)$$

Apart from the first term on the right-hand side, this result is equivalent to Eq. (27), which was derived using the principle of virtual work. Isotropic contributions to the stress tensor do not affect the compliance with the stress-optical rule, nor the consistency between small deformations and the Green-Kubo relation [5]. Since the relaxation modulus is related to deviatoric stresses, and the equilibrium PP-length distribution is not determined by the stress tensor at all [18], both remain consistent with results from multi-chain models and simulations. Thus all four criteria, discussed in Sec. ID, remain satisfied.

A few interesting observations can be made regarding the derivation of the stress tensor:

- It was shown in Sec. IIB that the anisotropic part of the IMSM stress tensor has a contribution from the virtual springs. For the AMSM, if the ESFs do not follow the generalized Ronca-Allegra dynamics, there is also a contribution from the confinement potentials. These two types of “virtual” stresses, which cause violation of the stress-optical rule and inconsistency with the multi-chain relaxation modulus, originate from the terms involving derivatives of the chain free energy on the last two lines of Eq. (69). With the generalized Ronca-Allegra dynamics, these terms cancel each other, as shown in Eq. (73). No cancellation occurs between contributions to the isotropic part of the stress tensor, which originate from the terms involving derivatives of the probability density in Eq. (69). Since these isotropic terms do not lead to any violations, the Ronca-Allegra dynamics are necessary and sufficient for simultaneous compliance with all four criteria.

- The stress tensor can also be derived using the principle of virtual work. This yields only the anisotropic part of the stress tensor. Similar to the GENERIC derivation, contributions from the virtual springs and the confinement potentials cancel each other when the anisotropy of ESFs is described by the generalized Ronca-Allegra dynamics, as shown by Schieber *et al.* [5] and in our Sec. II C.
- Left-multiplying the energy gradient, given in Eq. (55), by the Poisson matrix \mathbf{L} , given in Eq. (61), yields the reversible dynamics of the state variables \mathbf{x} . Because the stress tensor appears on the second and third lines of \mathbf{L} , it has reversible contributions to the evolution equations for the momentum density and the internal energy density. These contributions are of the form $-\nabla \cdot \mathbf{\Pi}$ and $-\boldsymbol{\kappa} : \mathbf{\Pi}$, respectively [23, 94]. This means that, in general, the virtual springs and the anisotropic confinement potentials influence the momentum and energy of the system. For an incompressible material, $\boldsymbol{\kappa} : \boldsymbol{\delta} = 0$ and only the anisotropic part of the stress tensor contributes to the energy balance. Hence, with Ronca-Allegra dynamics, ESFs do not affect the energy of an incompressible system.
- The isotropic part of the stress tensor is proportional to the number of vectorial variables whose equation of motion has an affine component. These variables appear in the \mathbf{L}_{42} element of the Poisson matrix, Eq. (62), and due to the antisymmetry condition and the Jacobi identity, also in the \mathbf{L}_{24} element, Eq. (63). Thus they contribute to the reversible part of the momentum balance. It is straightforward to show that this is true for dif-

ferent versions of the model. For the FSM, which does not have the $Z - 1$ virtual springs and the $3Z - 3$ vectors $\{\mathbf{a}_i\}$ describing the confinement potentials, the isotropic part of the stress tensor is $k_B T n_c \langle Z \rangle \boldsymbol{\delta}$ instead of $k_B T n_c (5 \langle Z \rangle - 4) \boldsymbol{\delta}$. If the dangling ends are coarse-grained out, the isotropic stress due to the strands changes from $k_B T n_c \langle Z \rangle \boldsymbol{\delta}$ to $k_B T n_c \langle (Z - 2) \mathcal{H}(Z - 2) \rangle \boldsymbol{\delta}$, while the contributions from the virtual springs and the confinement potentials stay the same. Here $\mathcal{H}(x) = \sum_{y=1}^{\infty} \delta_{xy}$ is a discrete version of the Heaviside function $H(x)$. If information about the absolute spatial position of the chain is included, as in the variable space Ω^+ given in Eq. (29), the isotropic stress increases by $k_B T n_c \boldsymbol{\delta}$.

- Whether the functional derivatives of the total energy E and the total entropy S are constrained or unconstrained has no effect on the resulting stress tensor. This is proven in Appendix A.

2. Irreversible dynamics

The second term on the right-hand side of the GENERIC, Eq. (38), yields the irreversible dynamics of the system. The friction matrix \mathbf{M} can be constructed by first entering those elements that produce what is known of the irreversible dynamics, and then using the requirements that \mathbf{M} must be symmetric and positive semidefinite, and must fulfill the degeneracy condition, Eq. (40), to find the other elements. This was demonstrated for the Hookean dumbbell model by Öttinger and Grmela [23] and for the FSM by Schieber [94]. We follow the same procedure for the AMSM. The friction matrix then has the form

$$\mathbf{M} = \begin{pmatrix} 0 & \mathbf{0} & 0 & 0 \\ \mathbf{0} & -(\nabla \eta_s T \nabla)^\dagger - \boldsymbol{\delta} \nabla \cdot \eta_s T \nabla & \nabla \cdot \eta_s T \dot{\boldsymbol{\gamma}} & \mathbf{0} \\ 0 & -\eta_s T \dot{\boldsymbol{\gamma}} \cdot \nabla & \frac{1}{2} \eta_s T \dot{\boldsymbol{\gamma}} : \dot{\boldsymbol{\gamma}} - \nabla \cdot \boldsymbol{\lambda} T^2 \cdot \nabla & 0 \\ 0 & \mathbf{0} & 0 & \mathbf{M}_{44} \end{pmatrix}, \quad (75)$$

where η_s is the viscosity of the solvent (if present) or related to the short-time-scale dynamics of the melt, $\dot{\boldsymbol{\gamma}} = \boldsymbol{\kappa} + \boldsymbol{\kappa}^\dagger$ equals twice the symmetric part of the velocity gradient tensor, and $\boldsymbol{\lambda}$ is the thermal conductivity tensor. The 2×2 block in the middle of \mathbf{M} is the same as in classical hydrodynamics [23, 113].

The probability density for the chain conformation evolves according to the differential Chapman-Kolmogorov equation, Eq. (6), which is the sum of a linear Fokker-Planck equation and a master equation. The element in the lower right corner of \mathbf{M} is therefore written as

$$\mathbf{M}_{44} = \mathbf{M}_{44}^{\text{FP}} + \mathbf{M}_{44}^{\text{ME}}. \quad (76)$$

The Fokker-Planck part is given by Eq. (37), with the last term modified as in Eq. (47) if the confinement potentials are described by vectors $\{\mathbf{a}_i^\alpha\}$ instead of tensors $\{\mathbf{n}_i\}$. The irreversible dynamics in the Fokker-Planck equation are due to the diffusive motion of the slip-links, and are generated by

$$\mathbf{M}_{44}^{\text{FP}} = -\frac{1}{k_B \zeta} \left[\sum_{i=1}^Z \frac{\partial}{\partial \mathbf{Q}_i} \cdot p(\Omega_a) \left(\sum_{j=1}^Z A_{ij} \frac{\partial}{\partial \mathbf{Q}_j} + \sum_{j=1}^{Z-1} B_{ij} \frac{\partial}{\partial \mathbf{X}_j} \right) + \sum_{i=1}^{Z-1} \frac{\partial}{\partial \mathbf{X}_i} \cdot p(\Omega_a) \left(\sum_{j=1}^Z B_{ji} \frac{\partial}{\partial \mathbf{Q}_j} + \frac{\partial}{\partial \mathbf{X}_i} \right) \right]. \quad (77)$$

Ignoring the virtual springs, this is similar to M_{44}^{FP} in an older version of the FSM [94]. However, different physics are implied: whereas Schieber [94] used diffusive motion of the slip-links to mimic constraint dynamics, we use it to describe ESFs.

The current version of the FSM employs a rigorous formulation of entanglement creation and destruction events as discrete jump processes [6, 10]. This means that constraint dynamics are contained in the master-equation part of Eq. (6). Detailed balance is satisfied by using transition rates of the form

$$W(\Omega_a|\Omega'_a) = \Delta(\Omega_a, \Omega'_a) \sqrt{\frac{p_{\text{eq}}(\Omega_a)}{p_{\text{eq}}(\Omega'_a)}}, \quad (78)$$

where the function Δ is nonnegative and symmetric in its arguments [114]. The transition rate consists of additive contributions from sliding dynamics of Kuhn steps, entanglement creation and destruction by sliding dynamics, and entanglement creation and destruction by constraint dynamics. Schieber [94] showed that

$$M_{44}^{\text{ME}} = \frac{1}{k_B} \int \frac{\Delta(\Omega_a, \Omega'_a)}{\sqrt{p_{\text{eq}}(\Omega_a)p_{\text{eq}}(\Omega'_a)}} \left[\frac{p(\Omega'_a)p_{\text{eq}}(\Omega_a) - p(\Omega_a)p_{\text{eq}}(\Omega'_a)}{\log\left(\frac{p(\Omega'_a)p_{\text{eq}}(\Omega_a)}{p(\Omega_a)p_{\text{eq}}(\Omega'_a)}\right)} \right] [\delta(\Omega_a - \Omega'_a) - \delta(\Omega'_a - \Omega_a)] d\Omega'_a \quad (79)$$

produces the master equation and is consistent with the GENERIC structure. Here the shorthand

$$\begin{aligned} \delta(\Omega_a - \Omega'_a) \equiv & \delta_{Z,Z'} \prod_{i=1}^Z \delta_{N_i, N'_i} \delta(\mathbf{Q}_i - \mathbf{Q}'_i) \prod_{j=1}^{Z-1} \delta(\mathbf{X}_j - \mathbf{X}'_j) \\ & \times \prod_{\alpha=1}^3 \delta(\mathbf{a}_j^\alpha - \mathbf{a}'_j^\alpha) \end{aligned} \quad (80)$$

is used. Although the second factor in the integrand of Eq. (79) has a singularity at $\Omega_a = \Omega'_a$, its limit as $\Omega_a \rightarrow \Omega'_a$ exists:

$$\lim_{\Omega_a \rightarrow \Omega'_a} \frac{p(\Omega'_a)p_{\text{eq}}(\Omega_a) - p(\Omega_a)p_{\text{eq}}(\Omega'_a)}{\log\left(\frac{p(\Omega'_a)p_{\text{eq}}(\Omega_a)}{p(\Omega_a)p_{\text{eq}}(\Omega'_a)}\right)} = p(\Omega_a)p_{\text{eq}}(\Omega_a). \quad (81)$$

Equation (79) was inspired by the friction matrix in the original GENERIC formulation of Boltzmann's kinetic equation by Öttinger [115]. This friction matrix was obtained empirically, i.e., it was chosen such that it would generate the known dynamics, while satisfying the GENERIC conditions of degeneracy [Eq. (40)], symmetry, and positive semidefiniteness of \mathbf{M} . Later, by thermodynamically consistent coarse-graining from an atomistic level of description, Öttinger [116] derived a different friction matrix for the Boltzmann equation, which is not symmetric. A similar approach could be followed here. On the other hand, recent work by Öttinger [117] on thermodynamically consistent model reduction suggests a fundamental basis for the friction matrix given in Eq. (79). In model reduction, one eliminates degrees of freedom by projecting the dynamics of the system onto a reduced set of variables, which are functions of the original, larger set of variables. This is different from coarse-graining, which typically eliminates fast variables by time- or ensemble-averaging. For the one-dimensional linear Fokker-Planck equation describing the

Kramers barrier crossing problem, Öttinger [117] showed that model reduction leads to a master equation, which is generated by a friction matrix analogous to Eq. (79).

Finally, we note that irreversible dynamics due to jump processes are described more naturally by dissipation potentials than by friction matrices. These two alternative formulations of GENERIC irreversible dynamics have been discussed and compared in detail by Grmela and Öttinger [22], Hütter and Svendsen [34], and Öttinger [118].

With the Poisson matrix \mathbf{L} , the friction matrix \mathbf{M} , and the energy and entropy gradients known, Eq. (38) gives the evolution equations for the state variables. The first three are the well-known balance equations for mass, momentum, and internal energy [23]. The fourth is the differential Chapman-Kolmogorov equation for the probability density, which for the AMSM is given by Eq. (6), Eq. (37) or (47), and expressions for the transition rates of all the jump processes [6, 10].

IV. SUMMARY AND OUTLOOK

Our work shows that, when entanglement spatial fluctuations (ESFs) are incorporated in the slip-link model, simultaneous compliance with four fundamental consistency criteria [5] is achieved only if the time evolution of the directionality of ESFs is upper-convected. This time evolution is analogous to the dynamics of node fluctuations in the cross-linked network model of Ronca and Allegra [80], but it is applicable to polymer systems containing cross-links, entanglements, or both, under arbitrary flow conditions. An anisotropic mobile slip-link model (AMSM), based on these generalized Ronca-Allegra dynamics, was proposed, and its compliance with three of the four criteria was demonstrated previously [5, 18]. The present work provides a rigorous proof that the AMSM also satisfies the remaining criterion: con-

sistency with nonequilibrium thermodynamics. To the best of our knowledge, no other single-chain mean-field entanglement model has achieved this.

The detailed agreement with multi-chain simulations (another one of the four criteria) allows all the parameters of the AMSM to be determined *ab initio* [18, 19]. The AMSM can be coarse-grained to less detailed levels of description by averaging over fluctuations. The parameters of each model are mapped onto a reduced set of modified parameters for the next less detailed model, thus preserving the possibility of *ab initio* rheology predictions at each level [13, 19]. The least detailed member of the DSM family of models, namely the clustered fixed slip-link model (CFSM), is obtained not by averaging over fluctuations, but by exploiting universality in the rheology of flexible polymers with the same average number of entanglements per chain [12, 13]. The CFSM has two parameters, and it has recently been shown that they can both be estimated from the crossover between the storage and loss moduli [119].

Other opportunities exist in coarse-graining of these slip-link models by taking the continuous limit of (functions of) their discrete variables, to create a range of tube models at different levels of description. Recent work on this type of coarse-graining of the isotropic mobile slip-link model (IMSM) [81] can be taken as a starting point. An interesting connection between the AMSM and Öttinger's thermodynamically consistent tube model with anisotropic tube cross sections [112, 120], which was pointed out by Schieber *et al.* [5], might be useful to direct future efforts in coarse-graining of the AMSM to a tube-like level of description.

Even if further coarse-graining is not possible, current implementations of the slip-link model are sufficiently inexpensive to allow the prediction of flows in complex geometries [121, 122]. Since these coarse-grained versions are closely integrated with the more detailed AMSM, and their parameters can be determined from those obtained for the AMSM [13, 19], there now exists a strong connection between atomistic models and flow predictions, with each step on firm thermodynamic footing.

ACKNOWLEDGMENTS

The authors are grateful to the Army Research Office for funding through grants W911NF-08-2-0058 and W911NF-09-2-0071.

APPENDIX A: CANCELLATION OF CONSTRAINTS IN THE STRESS TENSOR DERIVATION

The degeneracy condition for the Poisson matrix, Eq. (39), yields an expression from which the entropic stress tensor $\mathbf{\Pi}$ can be derived. In Eq. (64), this expression is given explicitly for the anisotropic mobile slip-link

model. In a more general form, it reads

$$\begin{aligned} \nabla \cdot \left(\frac{\mathbf{\Pi}}{T} \right) = & -\rho \nabla \frac{\delta S_c}{\delta \rho} - \int p(\Omega) \nabla \frac{\delta S_c}{\delta p(\Omega)} d\Omega \\ & + \nabla \int p(\Omega) \frac{\delta S_c}{\delta p(\Omega)} d\Omega + \mathbf{L}_{24}^{\text{FP}} * \frac{\delta S_c}{\delta p(\Omega)}, \end{aligned} \quad (\text{A1})$$

where $-\mathbf{L}_{24}^{\text{FP}}$ represents the last term in Eq. (63). The cancellation of the first two terms on the right-hand side of Eq. (64), due to Eqs. (65) and (66), has already been accounted for in Eq. (A1).

The functional derivative with respect to the mass density has the form

$$\frac{\delta S_c}{\delta \rho} = \frac{\delta_u S_c}{\delta_u \rho} - \frac{1}{m} \int \rho \frac{\delta_u S_c}{\delta_u \rho} d\mathbf{r}, \quad (\text{A2})$$

as derived in the Supplemental Material [111]. Here the symbol δ_u indicates that no constraint is imposed on variations when calculating the functional derivative. The last term in Eq. (A2) compensates for violations of the mass-conservation constraint, Eq. (51). Since this term is an integral over the volume of the system, it vanishes when operated on by the gradient in the first term on the right-hand side of Eq. (A1), hence

$$\nabla \frac{\delta S_c}{\delta \rho} = \nabla \frac{\delta_u S_c}{\delta_u \rho}. \quad (\text{A3})$$

Similarly, in the functional derivative with respect to the probability density,

$$\frac{\delta S_c}{\delta p(\Omega)} = \frac{\delta_u S_c}{\delta_u p(\Omega)} - \int p(\Omega) \frac{\delta_u S_c}{\delta_u p(\Omega)} d\Omega, \quad (\text{A4})$$

the last term compensates for violations of the normalization constraint, Eq. (52). Since this term is an integral over all possible conformations, it vanishes when operated on by $\mathbf{L}_{24}^{\text{FP}}$, which takes derivatives with respect to the conformational variables. Thus the last term on the right-hand side of Eq. (A1) becomes

$$\mathbf{L}_{24}^{\text{FP}} * \frac{\delta S_c}{\delta p(\Omega)} = \mathbf{L}_{24}^{\text{FP}} * \frac{\delta_u S_c}{\delta_u p(\Omega)}. \quad (\text{A5})$$

When Eq. (A4) is substituted into the second term and the third term on the right-hand side of Eq. (A1), there are two possible cancellations: either the two contributions from the normalization constraint cancel each other out, or the entire third term vanishes because

$$\int p(\Omega) \frac{\delta S_c}{\delta p(\Omega)} d\Omega = 0, \quad (\text{A6})$$

while the second term remains. Either way, the final result is

$$\begin{aligned} \nabla \cdot \left(\frac{\mathbf{\Pi}}{T} \right) = & -\rho \nabla \frac{\delta_u S_c}{\delta_u \rho} - \int p(\Omega) \nabla \frac{\delta_u S_c}{\delta_u p(\Omega)} d\Omega \\ & + \nabla \int p(\Omega) \frac{\delta_u S_c}{\delta_u p(\Omega)} d\Omega + \mathbf{L}_{24}^{\text{FP}} * \frac{\delta_u S_c}{\delta_u p(\Omega)}. \end{aligned} \quad (\text{A7})$$

This is just Eq. (A1) with all constrained functional derivatives replaced by unconstrained ones. Since the contributions from the two constraints (conservation of mass and normalization of the probability density) vanish independently, the correct stress tensor is obtained whether we account for both constraints, ignore one or the other, or ignore both of them. This explains why our results are consistent with those found in previous works, even though some did not account for any constraints and others accounted only for normalization of the probability density. One small difference is due to an error in a previous publication, which we correct in Appendix B.

APPENDIX B: REVIEW OF STRESS TENSOR DERIVATIONS IN PREVIOUS WORKS

For comparison with the work of Öttinger and Grmela [23], we also derive the stress tensor using the state variables

$$\mathbf{x} = \begin{pmatrix} \rho(\mathbf{r}) \\ \mathbf{u}(\mathbf{r}) \\ \epsilon(\mathbf{r}) \\ \psi(\Omega; \mathbf{r}) \end{pmatrix}, \quad (\text{B1})$$

where $\psi(\Omega; \mathbf{r})$ is the probability density for the chain conformation, normalized to the number density of chains,

$$\int \psi(\Omega; \mathbf{r}) d\Omega = n_c(\rho(\mathbf{r})) = \frac{N_A \rho(\mathbf{r})}{M}. \quad (\text{B2})$$

Combined with the conservation of mass, Eq. (51), this gives

$$\iint \psi(\Omega; \mathbf{r}) d\Omega d\mathbf{r} = N_c = \frac{N_A m}{M}. \quad (\text{B3})$$

In Eqs. (B2) and (B3), the second equality is valid only for monodisperse melts. Modification of these expressions for polydisperse and/or diluted systems is straightforward, as explained in the main text after Eq. (13).

The derivation below shows that the same stress tensor is obtained whether we use $p(\Omega)$ or $\psi(\Omega)$ as a state variable, which is not surprising. A more interesting result is that the stress tensor reported by Öttinger and Grmela [23] contains a small error, whose source is identified here. Furthermore, we resolve an ambiguity in the work of Schieber [94] as to which state variables were used. As before, the notation is simplified by omitting all dependencies on the position \mathbf{r} .

Expressed in terms of the state variables in Eq. (B1), the probability density used elsewhere in this paper is

$$p(\rho, \psi(\Omega)) = \frac{\psi(\Omega)}{n_c(\rho)}. \quad (\text{B4})$$

Therefore, using Eq. (13) and the continuity equation,

$$\frac{\partial \rho}{\partial t} = -\nabla \cdot (\rho \mathbf{v}), \quad (\text{B5})$$

the differential Chapman-Kolmogorov equation for the chain conformation, Eq. (6), becomes

$$\begin{aligned} \frac{\partial \psi(\Omega)}{\partial t} = & -\nabla \cdot (\psi(\Omega) \mathbf{v}) + \mathcal{L}(\Omega) * \psi(\Omega) \\ & + \int [W(\Omega|\Omega')\psi(\Omega') - W(\Omega'\|\Omega)\psi(\Omega)] d\Omega'. \end{aligned} \quad (\text{B6})$$

For the AMSM, the Fokker-Planck operator $\mathcal{L}(\Omega)$ is given by Eq. (37) with $p(\Omega)$ replaced by $\psi(\Omega)$. The reversible dynamics, which include the convective term on the left-hand side of Eq. (B6) and the Fokker-Planck terms related to affine motions, are generated by the Poisson matrix element

$$\mathbf{L}_{42} = -\nabla \psi(\Omega) + \mathbf{L}_{42}^{\text{FP}}, \quad (\text{B7})$$

where $\mathbf{L}_{42}^{\text{FP}}$ is given by Eq. (62) with $p(\Omega)$ replaced by $\psi(\Omega)$. This requires

$$\mathbf{L}_{24} = -\psi(\Omega') \nabla + \mathbf{L}_{24}^{\text{FP}} \quad (\text{B8})$$

to preserve the antisymmetry and the Jacobian structure of \mathbf{L} [23]. Here $\mathbf{L}_{24}^{\text{FP}}$ is given by Eq. (63) with $p(\Omega)$ replaced by $\psi(\Omega)$.

The total energy and its gradient are the same as in Eqs. (48) and (55). The conformational part of the total entropy, Eq. (49), is now

$$S_c[\rho, \psi(\Omega)] = -k_B \iint \psi(\Omega) \log \left(\frac{\psi(\Omega)}{n_c(\rho) p_{\text{eq}}(\Omega)} \right) d\Omega d\mathbf{r} \quad (\text{B9})$$

with $p_{\text{eq}}(\Omega)$ as in Eq. (4). The unconstrained functional derivative of the conformational entropy with respect to the mass density is

$$\frac{\delta_{\mathbf{u}} S_c}{\delta_{\mathbf{u}} \rho} = k_B \frac{dn_c}{d\rho} = \frac{k_B N_A}{M}. \quad (\text{B10})$$

Again, the second equality is valid only for monodisperse melts, but generalization is straightforward. Substitution of Eq. (B10) into Eq. (A2) yields

$$\frac{\delta S_c}{\delta \rho} = 0. \quad (\text{B11})$$

The constrained functional derivative with respect to $\psi(\Omega)$ has the form

$$\frac{\delta S_c}{\delta \psi(\Omega)} = \frac{\delta_{\mathbf{u}} S_c}{\delta_{\mathbf{u}} \psi(\Omega)} - \frac{1}{N_c} \iint \psi(\Omega) \frac{\delta_{\mathbf{u}} S_c}{\delta_{\mathbf{u}} \psi(\Omega)} d\Omega d\mathbf{r}, \quad (\text{B12})$$

as can be derived using either of the two methods discussed in the Supplemental Material [111]. From Eq. (B9), we obtain

$$\frac{\delta_{\mathbf{u}} S_c}{\delta_{\mathbf{u}} \psi(\Omega)} = -k_B \log \left(\frac{\psi(\Omega)}{n_c(\rho) p_{\text{eq}}(\Omega)} \right) - k_B, \quad (\text{B13})$$

and hence

$$\begin{aligned} \frac{\delta S_c}{\delta \psi(\Omega)} &= -k_B \log \left(\frac{\psi(\Omega)}{n_c(\rho)p_{\text{eq}}(\Omega)} \right) \\ &+ \frac{k_B}{N_c} \iint \psi(\Omega) \log \left(\frac{\psi(\Omega)}{n_c(\rho)p_{\text{eq}}(\Omega)} \right) d\Omega dr. \end{aligned} \quad (\text{B14})$$

Now that the Poisson matrix and the entropy gradient have been specified, the degeneracy condition, Eq. (39), can be used to obtain the stress tensor $\mathbf{\Pi}$. We find

$$\begin{aligned} \nabla \cdot \left(\frac{\mathbf{\Pi}}{T} \right) &= - \int \psi(\Omega) \nabla \frac{\delta S_c}{\delta \psi(\Omega)} d\Omega + \mathbf{L}_{24}^{\text{FP}} * \frac{\delta S_c}{\delta \psi(\Omega)} \\ &= k_B \int \psi(\Omega) \nabla \log \left(\frac{\psi(\Omega)}{n_c(\rho)p_{\text{eq}}(\Omega)} \right) d\Omega \\ &+ \mathbf{L}_{24}^{\text{FP}} * \frac{\delta_u S_c}{\delta_u \psi(\Omega)}. \end{aligned} \quad (\text{B15})$$

The first term on the right-hand side can be written as

$$\begin{aligned} k_B \int \psi(\Omega) \left[\frac{\nabla \psi(\Omega)}{\psi(\Omega)} - \frac{\nabla n_c(\rho)}{n_c(\rho)} + \nabla \left(\frac{F(\Omega)}{k_B T} \right) \right] d\Omega \\ = k_B \int \psi(\Omega) \nabla \left(\frac{F(\Omega)}{k_B T} \right) d\Omega, \end{aligned} \quad (\text{B16})$$

where the first two terms cancel one another due to the normalization of $\psi(\Omega)$, Eq. (B2). Assuming that the chain free energy is proportional to the temperature, the stress tensor is then defined by

$$\nabla \cdot \left(\frac{\mathbf{\Pi}}{T} \right) = \mathbf{L}_{24}^{\text{FP}} * \frac{\delta_u S_c}{\delta_u \psi(\Omega)}. \quad (\text{B17})$$

The remaining derivation is analogous to the one in Sec. III A 1 and leads to Eq. (74) for the stress tensor.

For an unentangled polymer, $Z = 1$ and $\Omega = \{\mathbf{Q}\}$, where \mathbf{Q} is the chain end-to-end vector. Eq. (74) then becomes

$$\mathbf{\Pi} = k_B T n_c(\rho) \delta - n_c(\rho) \left\langle \mathbf{Q} \frac{\partial F(\mathbf{Q})}{\partial \mathbf{Q}} \right\rangle. \quad (\text{B18})$$

This is similar to Eq. (55) of Öttinger and Grmela [23], only their isotropic term is larger than ours by a factor of 2. Comparing the conformational part of the entropy in their Eq. (49) to our Eq. (B9), it becomes clear that they missed the factor $n_c(\rho)$ in the denominator of the logarithm. If we were to ignore that factor, the second term in Eq. (B16) would disappear and thus the first term in Eq. (B16) would not be canceled out. Consequently, we would obtain $2k_B T n_c(\rho) \delta$ as the isotropic contribution to the stress, just like Öttinger and Grmela [23].

In the GENERIC formulation of the FSM by Schieber [94], the probability density, called $p(\Omega)$, is not consistently normalized in the same way. In his Sec. 2, Schieber presents the differential Chapman-Kolmogorov equation and the expression for $p_{\text{eq}}(\Omega)$. These are consistent with our Eqs. (6) and (4), respectively. This means that $p(\Omega)$ is normalized to 1. However, in Schieber's Sec. 3, the expressions for the conformational entropy, its gradient, and the Poisson matrix elements \mathbf{L}_{42} and \mathbf{L}_{24} imply that $p(\Omega)$ is normalized to the chain number density, like $\psi(\Omega)$ in this appendix and in the work of Öttinger and Grmela [23]. This also clarifies the meaning of the $-S$ appearing in Schieber's Eq. (13) for the entropy gradient, which should be replaced by the second term on the right-hand side of our Eq. (B14).

In the version of the FSM used by Schieber [94], the dangling ends are coarse-grained out. Therefore they do not carry any stress and Eq. (74) becomes

$$\begin{aligned} \mathbf{\Pi} &= k_B T n_c(\rho) \langle (Z - 2) \mathcal{H}(Z - 2) \rangle \delta \\ &- n_c(\rho) \left\langle \sum_{i=2}^{Z-1} \mathbf{Q}_i \frac{\partial F_s}{\partial \mathbf{Q}_i} \right\rangle. \end{aligned} \quad (\text{B19})$$

The Heaviside function \mathcal{H} accounts for the fact that unentangled and once-entangled chains do not carry any stress in this model. Besides two minor differences with Schieber's Eq. (17), namely a sign error originating from his Eq. (16) and a misprint of the summation sign outside of the angle brackets, which denote the ensemble average, there is also a difference in the magnitude of the isotropic contribution to the stress tensor. In Schieber's Eq. (17), this term is proportional to $\langle Z \rangle - 1$ because he omitted the factor $n_c(\rho)$ in the denominator of the logarithmic term in the conformational entropy. This is the same error that was made by Öttinger and Grmela [23], as explained above.

-
- | | |
|---|--|
| [1] F. Bueche, <i>J. Chem. Phys.</i> 20 , 1959 (1952). | 7504 (2009). |
| [2] W. W. Graessley, <i>J. Chem. Phys.</i> 43 , 2696 (1965). | [7] R. N. Khaliullin and J. D. Schieber, <i>Macromolecules</i> 43 , 6202 (2010). |
| [3] S. F. Edwards, <i>Proc. Phys. Soc.</i> 92 , 9 (1967). | [8] E. Pilyugina, M. Andreev, and J. D. Schieber, <i>Macromolecules</i> 45 , 5728 (2012). |
| [4] S. D. Anogiannakis, C. Tzoumanekas, and D. N. Theodorou, <i>Macromolecules</i> 45 , 9475 (2012). | [9] M. K. Jensen, R. Khaliullin, and J. D. Schieber, <i>Rheol. Acta</i> 51 , 21 (2012). |
| [5] J. D. Schieber, T. Indei, and R. J. A. Steenbakkers, <i>Polymers</i> 5 , 643 (2013). | [10] M. Andreev, R. N. Khaliullin, R. J. A. Steenbakkers, |
| [6] R. N. Khaliullin and J. D. Schieber, <i>Macromolecules</i> 42 , | |

- and J. D. Schieber, *J. Rheol.* **57**, 535 (2013).
- [11] M. Katzarova, M. Andreev, Y. R. Sliozberg, R. A. Mrozek, J. L. Lenhart, J. W. Andzelm, and J. D. Schieber, *AIChE J.* **60**, 1372 (2014).
- [12] M. Andreev, H. Feng, L. Yang, and J. D. Schieber, *J. Rheol.* **58**, 723 (2014).
- [13] J. D. Schieber and M. Andreev, *Annu. Rev. Chem. Biomol. Eng.* **5**, 367 (2014).
- [14] P. S. Desai, B.-G. Kang, M. Katzarova, R. Hall, Q. Huang, S. Lee, M. Shivokhin, T. Chang, D. C. Venerus, J. Mays, J. D. Schieber, and R. G. Larson, *Macromolecules* **49**, 4964 (2016).
- [15] M. Katzarova, T. Kashyap, J. D. Schieber, and D. C. Venerus, *Rheol. Acta* **57**, 327 (2018).
- [16] N. E. Valadez-Pérez, K. Taletskiy, J. D. Schieber, and M. Shivokhin, *Polymers* **10**, 908 (2018).
- [17] K. Taletskiy, T. A. Tervoort, and J. D. Schieber, *J. Rheol.* **62**, 1331 (2018).
- [18] R. J. A. Steenbakkens, C. Tzoumanekas, Y. Li, W. K. Liu, M. Kröger, and J. D. Schieber, *New J. Phys.* **16**, 015027 (2014).
- [19] D. Becerra, A. Córdoba, M. Katzarova, M. Andreev, D. C. Venerus, and J. D. Schieber, *J. Rheol.* **64**, 1035 (2020).
- [20] A. Bach, K. Almdal, H. K. Rasmussen, and O. Hassager, *Macromolecules* **36**, 5174 (2003).
- [21] A. N. Kaufman, *Phys. Lett. A* **100**, 419 (1984).
- [22] M. Grmela and H. C. Öttinger, *Phys. Rev. E* **56**, 6620 (1997).
- [23] H. C. Öttinger and M. Grmela, *Phys. Rev. E* **56**, 6633 (1997).
- [24] H. C. Öttinger, *Phys. Rev. E* **57**, 1416 (1998).
- [25] H. C. Öttinger, *Beyond Equilibrium Thermodynamics* (Wiley-Interscience, Hoboken, NJ, 2005).
- [26] B. J. Edwards, H. C. Öttinger, and R. J. J. Jongschaap, *J. Non-Equilib. Thermodyn.* **22**, 356 (1997).
- [27] B. J. Edwards, *J. Non-Equilib. Thermodyn.* **23**, 301 (1998).
- [28] W. Muschik, S. Gümbel, M. Kröger, and H. C. Öttinger, *Physica A* **285**, 448 (2000).
- [29] D. Jou and J. Casas-Vázquez, *J. Non-Newton. Fluid Mech.* **96**, 77 (2001).
- [30] W. Muschik, C. Papenfuss, and H. Ehrentraut, *J. Non-Newton. Fluid Mech.* **96**, 255 (2001).
- [31] R. Jongschaap and H. C. Öttinger, *J. Non-Newton. Fluid Mech.* **120**, 3 (2004).
- [32] H. C. Öttinger, *J. Stat. Phys.* **138**, 1067 (2010).
- [33] A. Favache, D. Dochain, and B. Maschke, *Chem. Eng. Sci.* **65**, 5204 (2010).
- [34] M. Hütter and B. Svendsen, *Contin. Mech. Thermodyn.* **25**, 803 (2013).
- [35] A. Montefusco, F. Consonni, and G. P. Beretta, *Phys. Rev. E* **91**, 042138 (2015).
- [36] Y.-H. Lin, *Macromolecules* **20**, 3080 (1987).
- [37] T. A. Kavassalis and J. Noolandi, *Phys. Rev. Lett.* **59**, 2674 (1987).
- [38] T. A. Kavassalis and J. Noolandi, *Macromolecules* **21**, 2869 (1988).
- [39] T. A. Kavassalis and J. Noolandi, *Macromolecules* **22**, 2709 (1989).
- [40] L. J. Fetters, D. J. Lohse, D. Richter, T. A. Witten, and A. Zirkel, *Macromolecules* **27**, 4639 (1994).
- [41] L. J. Fetters, D. J. Lohse, and W. W. Graessley, *J. Polym. Sci., Part B: Polym. Phys.* **37**, 1023 (1999).
- [42] L. J. Fetters, D. J. Lohse, S. T. Milner, and W. W. Graessley, *Macromolecules* **32**, 6847 (1999).
- [43] R. Krishnamoorti, W. W. Graessley, A. Zirkel, D. Richter, N. Hadjichristidis, L. J. Fetters, and D. J. Lohse, *J. Polym. Sci., Part B: Polym. Phys.* **40**, 1768 (2002).
- [44] M. Abdel-Goad, W. Pyckhout-Hintzen, S. Kahle, J. Allgaier, D. Richter, and L. J. Fetters, *Macromolecules* **37**, 8135 (2004).
- [45] M. Doi and S. F. Edwards, *The Theory of Polymer Dynamics* (Oxford University Press, Oxford, UK, 1986).
- [46] A. E. Likhtman and T. C. B. McLeish, *Macromolecules* **35**, 6332 (2002).
- [47] R. G. Larson, T. Sridhar, L. G. Leal, G. H. McKinley, A. E. Likhtman, and T. C. B. McLeish, *J. Rheol.* **47**, 809 (2003).
- [48] J. D. Schieber and K. Horio, *J. Chem. Phys.* **132**, 074905 (2010).
- [49] R. Everaers, S. K. Sukumaran, G. S. Grest, C. Svaneborg, A. Sivasubramanian, and K. Kremer, *Science* **303**, 823 (2004).
- [50] S. Shanbhag and R. G. Larson, *Phys. Rev. Lett.* **94**, 076001 (2005).
- [51] M. Kröger, *Comput. Phys. Commun.* **168**, 209 (2005).
- [52] Q. Zhou and R. G. Larson, *Macromolecules* **38**, 5761 (2005).
- [53] C. Tzoumanekas and D. N. Theodorou, *Macromolecules* **39**, 4592 (2006).
- [54] S. Shanbhag and M. Kröger, *Macromolecules* **40**, 2897 (2007).
- [55] M. Doi and S. F. Edwards, *J. Chem. Soc., Faraday Trans. 2* **74**, 1789 (1978).
- [56] M. Doi and S. F. Edwards, *J. Chem. Soc., Faraday Trans. 2* **74**, 1802 (1978).
- [57] M. Doi and S. F. Edwards, *J. Chem. Soc., Faraday Trans. 2* **74**, 1818 (1978).
- [58] M. Doi and S. F. Edwards, *J. Chem. Soc., Faraday Trans. 2* **75**, 38 (1979).
- [59] K. Foteinopoulou, N. C. Karayiannis, V. G. Mavrantzas, and M. Kröger, *Macromolecules* **39**, 4207 (2006).
- [60] K. Kamio, K. Moorthi, and D. N. Theodorou, *Macromolecules* **40**, 710 (2007).
- [61] T. Spyriouni, C. Tzoumanekas, D. Theodorou, F. Müller-Plathe, and G. Milano, *Macromolecules* **40**, 3876 (2007).
- [62] V. A. Harmandaris and K. Kremer, *Macromolecules* **42**, 791 (2009).
- [63] C. Tzoumanekas, F. Lahmar, B. Rousseau, and D. N. Theodorou, *Macromolecules* **42**, 7474 (2009).
- [64] R. S. Hoy, K. Foteinopoulou, and M. Kröger, *Phys. Rev. E* **80**, 031803 (2009).
- [65] G. N. Toepperwein, N. C. Karayiannis, R. A. Riggleman, M. Kröger, and J. J. de Pablo, *Macromolecules* **44**, 1034 (2011).
- [66] P. S. Stephanou, C. Baig, G. Tsolou, V. G. Mavrantzas, and M. Kröger, *J. Chem. Phys.* **132**, 124904 (2010).
- [67] C. Baig, P. S. Stephanou, G. Tsolou, V. G. Mavrantzas, and M. Kröger, *Macromolecules* **43**, 8239 (2010).
- [68] P. S. Stephanou, C. Baig, and V. G. Mavrantzas, *Soft Matter* **7**, 380 (2011).
- [69] P. S. Stephanou, C. Baig, and V. G. Mavrantzas, *Macromol. Theory Simul.* **20**, 752 (2011).

- [70] P. S. Stephanou and V. G. Mavrantzas, *J. Non-Newton. Fluid Mech.* **200**, 111 (2013).
- [71] W. Bisbee, J. Qin, and S. T. Milner, *Macromolecules* **44**, 8972 (2011).
- [72] A. E. Likhtman, *Soft Matter* **10**, 1895 (2014).
- [73] A. E. Likhtman and M. Ponmurugan, *Macromolecules* **47**, 1470 (2014).
- [74] N. Uchida, G. S. Grest, and R. Everaers, *J. Chem. Phys.* **128**, 044902 (2008).
- [75] J. D. Schieber, *J. Chem. Phys.* **118**, 5162 (2003).
- [76] R. N. Khaliullin and J. D. Schieber, *Phys. Rev. Lett.* **100**, 188302 (2008).
- [77] G. G. Fuller, *Optical Rheometry of Complex Fluids*, Topics in Chemical Engineering (Oxford University Press, New York, 1995).
- [78] C. Luap, C. Müller, T. Schweizer, and D. C. Venerus, *Rheol. Acta* **45**, 83 (2005).
- [79] R. Kubo, *J. Phys. Soc. Jpn.* **12**, 570 (1957).
- [80] G. Ronca and G. Allegra, *J. Chem. Phys.* **63**, 4990 (1975).
- [81] R. J. A. Steenbakkers and J. D. Schieber, *J. Chem. Phys.* **137**, 034901 (2012).
- [82] Y. Masubuchi, G. Ianniruberto, F. Greco, and G. Marrucci, *J. Chem. Phys.* **119**, 6925 (2003).
- [83] J. A. Duizer, Ph.D. thesis, Rijksuniversiteit Leiden (1965).
- [84] W. W. Graessley, *Macromolecules* **8**, 186 (1975).
- [85] W. W. Graessley, *Macromolecules* **8**, 865 (1975).
- [86] P. J. Flory, M. Gordon, and N. G. McCrum, *Proc. R. Soc. London, Ser. A* **351**, 351 (1976).
- [87] A. J. Staverman, *Adv. Polym. Sci.* **44**, 73 (1982).
- [88] A. Cohen, *Rheol. Acta* **30**, 270 (1991).
- [89] M. Kröger, *J. Non-Newton. Fluid Mech.* **223**, 77 (2015).
- [90] B. C. Marchi and E. M. Arruda, *Rheol. Acta* **54**, 887 (2015).
- [91] R. Jedynek, *Math. Mech. Solids* **24**, 1992 (2015).
- [92] M. A. Biot, *Phys. Rev.* **97**, 1463 (1955).
- [93] M. Doi, *J. Chem. Phys.* **79**, 5080 (1983).
- [94] J. D. Schieber, *J. Non-Equilib. Thermodyn.* **28**, 179 (2003).
- [95] A. E. Likhtman, *Macromolecules* **38**, 6128 (2005).
- [96] T. Indei, J. D. Schieber, and J. Takimoto, *Rheol. Acta* **51**, 1021 (2012).
- [97] J. Ramírez, S. K. Sukumaran, and A. E. Likhtman, *J. Chem. Phys.* **126**, 244904 (2007).
- [98] T. Indei, *Nihon Reoroji Gakkaishi* **42**, 111 (2014).
- [99] G. Heinrich, E. Straube, and G. Helmis, *Adv. Polym. Sci.* **85**, 33 (1988).
- [100] M. Rubinstein and S. Panyukov, *Macromolecules* **30**, 8036 (1997).
- [101] R. Everaers, *Eur. Phys. J. B* **4**, 341 (1998).
- [102] M. Rubinstein and S. Panyukov, *Macromolecules* **35**, 6670 (2002).
- [103] G. Allegra, S. Bontempelli, and G. Raos, *J. Chem. Phys.* **105**, 8352 (1996).
- [104] D. B. Adolf and J. G. Curro, *Macromolecules* **20**, 1646 (1987).
- [105] D. Adolf, *Macromolecules* **21**, 2249 (1988).
- [106] P. J. Flory, *J. Chem. Phys.* **66**, 5720 (1977).
- [107] C. W. Gardiner, *Handbook of Stochastic Methods for Physics, Chemistry and the Natural Sciences* (Springer, Berlin, 1982).
- [108] P. J. Morrison, *Rev. Mod. Phys.* **70**, 467 (1998).
- [109] I. M. Gelfand and S. V. Fomin, *Calculus of Variations* (Dover, Mineola, NY, 2000), translated and edited by R. A. Silverman.
- [110] H. C. Öttinger and A. N. Beris, *J. Chem. Phys.* **110**, 6593 (1999).
- [111] See Supplemental Material at [URL will be inserted by publisher] for a detailed comparison of the methods proposed by Öttinger and Beris [110] and Öttinger [25] to calculate constrained functional derivatives.
- [112] H. C. Öttinger, *J. Rheol.* **43**, 1461 (1999).
- [113] In the GENERIC derivation of the FSM by Schieber [94], the (2,2) element of \mathbf{M} is missing the second term, $-\delta\nabla \cdot \eta_s T \nabla$.
- [114] N. G. Van Kampen, *Stochastic Processes in Physics and Chemistry* (Elsevier, Amsterdam, 1992).
- [115] H. C. Öttinger, *J. Non-Equilib. Thermodyn.* **22**, 386 (1997).
- [116] H. C. Öttinger, *J. Non-Equilib. Thermodyn.* **27**, 105 (2002).
- [117] H. C. Öttinger, *Phys. Rev. E* **91**, 032147 (2015).
- [118] H. C. Öttinger, *J. Non-Equilib. Thermodyn.* **44**, 295 (2019).
- [119] M. Katzarova, L. Yang, M. Andreev, A. Córdoba, and J. D. Schieber, *Rheol. Acta* **54**, 169 (2015).
- [120] H. C. Öttinger, *J. Non-Newton. Fluid Mech.* **89**, 165 (2000).
- [121] M. Andreev and J. D. Schieber, *Macromolecules* **48**, 1606 (2015).
- [122] H. Feng, M. Andreev, E. Pilyugina, and J. D. Schieber, *Mol. Syst. Des. Eng.* **1**, 99 (2016).